Evolution of carbonation in cement blends incorporating thermally-mechanochemically activated low-kaolinite mixed-layer clays:

Cement and Concrete Research 208 (2026) 108322

Contents lists available at ScienceDirect

Cement and Concrete Research

journal homepage: www.elsevier.com/locate/cemconres

Evolution of carbonation in cement blends incorporating thermally-mechanochemically activated low-kaolinite mixed-layer clays: Insights into hydrate phase assemblage, C-A-S-H structure and porosity

Sahar Iftikhar [a,*,1], Ingemar Löfgren [a,b,2], Joao Figueira [c,3], Helen Jansson [a,1], Jelke Dijkstra [a,1], Arezou Babaahmadi [a,1]

[a] Chalmers University of Technology, Department of Architecture and Civil Engineering, Gothenburg, Sweden
[b] Thomas Concrete, Gothenburg, Sweden
[c] Department of Chemistry, Scilife Lab, Umeå University, Umeå, 90187, Sweden

ARTICLE INFO

Keywords:
Low-kaolinite
Carbonation
Hydrate phase assemblage
C-A-S-H decalcification
Pore structure evolution

ABSTRACT

Low-kaolinite clays represent a globally abundant resource for reducing clinker content, yet their durability remains poorly understood. This study examines the carbonation behavior of a clay blended binder incorporating 30 wt% of a thermally-mechanochemically activated 2:1 mixed-layer clay, with emphasis on hydrate assemblage evolution, C-A-S-H chemistry, and pore structure. Drying was decoupled from CO_2 exposure to distinguish physical conditioning from chemically driven carbonation damage, and curing duration was varied to access different hydrate states in this slow-reacting system. Carbonation proceeds through CH depletion, AFm/AFt destabilisation, and C-A-S-H decalcification; however, the extent of degradation depends strongly on the chemical maturity of the gel at the time of exposure. Binders carbonated after extended curing show markedly reduced decalcification (Ld ≈ 34% versus 92% in short-cured samples) and limited pore coarsening. Drying induces gel contraction and pore restructuring, but severe degradation occurs only when carbonation chemically decalcifies the gel. These results demonstrate that carbonation resistance in low-kaolinite binders is governed by hydrate assemblage evolution and chemical maturity of C-A-S-H, reflecting carbonation pathways distinct from those assumed for OPC and LC^3 systems.

1. Introduction

The growing focus on sustainable construction has driven increased interest in the use of supplementary cementitious materials (SCMs) as partial clinker replacements [1] offering a practical way to lower emissions while maintaining comparable performance. As traditional SCMs such as fly ash and slag become increasingly scarce, attention has shifted toward more abundant resources, particularly clays and limestone, which can be sourced worldwide and activated through calcination to provide significant pozzolanic reactivity. This shift has driven the development of limestone-calcined clay systems (LC^3), which combine calcined clay and limestone to achieve high reactivity and reduce clinker content by up to 50% while maintaining mechanical and durability performance [2]. Much of the early LC^3 research has centered on calcined clays containing at least 40% kaolinite, as kaolinite readily transforms into highly reactive metakaolin upon calcination and promotes the formation of carboaluminate phases that enhance strength and durability [3,4]. The hydration and durability of the traditional SCMs as well as kaolinitic clays is well studied [3–6]. However, such high-kaolinite clays are not representative of the majority of naturally occurring clay deposits worldwide. Most global clay resources contain less than 40% kaolinite and are instead dominated by a mix of less reactive 2:1 clay minerals (e.g., illite and smectite) and other non-clay minerals often considered impurities [7]. These types of clays are

* Corresponding author.
E-mail addresses: sahar.iftikhar@chalmers.se (S. Iftikhar), ingemar.lofgren@c-lab.se (I. Löfgren), joao.figueira@umu.se (J. Figueira), helen.jansson@chalmers.se (H. Jansson), jelke.dijkstra@chalmers.se (J. Dijkstra), arezou.ahmadi@chalmers.se (A. Babaahmadi).
[1] Chalmers University of Technology, Department of Architecture and Civil Engineering, SE-412 96 Gothenburg, Sweden.
[2] C-lab, Thomas Concrete Group, Ringogatan 12, SE-417 07 Gothenburg, Sweden.
[3] Department of Chemistry, Scilife Lab, Umeå University, Umeå, 90187, Sweden.

https://doi.org/10.1016/j.cemconres.2026.108322
Received 30 January 2026; Received in revised form 8 June 2026; Accepted 10 June 2026
Available online 7 July 2026

widely distributed across different geographical regions, including Northern and Central Europe [8,9], the United Kingdom [10], as well as in several regions of Southern Europe and parts of Africa [11,12], where kaolinite contents are often significantly lower, typically below 25%. The widespread occurrence of these clays makes them promising candidates for future SCMs, but their full potential pertaining to durability is not yet explored. Several studies have investigated the activation and hydration of 2:1 clays [13–15] while only a few have focused on their durability aspects [10,12]. This gap between commonly studied clays and those abundant worldwide highlights the need to broaden research toward lower-kaolinite, less reactive clays, ensuring durability and realistic global applicability in future standards and cement-replacement strategies.

Importantly, low-kaolinite 2:1 activated clays are not expected to simply reproduce the hydrate assemblages characteristic of kaolinite-rich LC^3 systems. Owing to their limited kaolinite content, these activated-clays supply substantially less reactive aluminum, which constrains the formation of AFm phases and alters the distribution of aluminum among hydration products. Previous work on the same binder system investigated in this study has demonstrated that, rather than forming discrete AFm phases, a large fraction of the available aluminum is incorporated directly into the C-A-S-H gel [16]. Consequently, the hydrate assemblage differs from both OPC and LC^3 systems, combining lower portlandite availability than OPC with a substantially reduced AFm buffering capacity relative to LC^3. The resulting C-A-S-H is also chemically distinct, with its structure and composition evolving gradually over extended curing periods. Such differences in hydrate chemistry suggest that carbonation in low-kaolinite 2:1 activated-clay binders may proceed through mechanisms that differ fundamentally from those established for OPC and LC^3 systems.

Carbonation is a degradation mechanism that occurs across all exposure classes and often governs the long-term performance of cementitious materials. While it has been extensively studied in the context of reinforcement depassivation, its influence on the hydrated cementitious matrix, particularly phase assemblage, C-A-S-H stability, and pore structure, remains insufficiently explored in modern low-clinker and activated-clay-based binders.

Carbonation in cementitious materials is one of the most influential physicochemical processes affecting both the phase assemblage and pore structure of hydrated binders. When atmospheric CO_2 diffuses through the pore network, it reacts with calcium-bearing phases such as portlandite (CH), calcium silicate hydrate (C–S–H), unhydrated clinker (C_3S and C_2S), and hydrated aluminate phases including AFm and AFt [17–19]. These reactions predominantly produce calcite [20,21], with minor occurrences of other calcium carbonate polymorphs such as aragonite and vaterite [22–26]. The mechanisms governing carbonation are strongly influenced by binder chemistry. These mechanisms, although reasonably well-understood for OPC, become even more intricate in blended binders. In ordinary Portland cement (OPC), carbonation is governed primarily by the reaction of CO_2 with portlandite [18]. In kaolinite-rich LC^3 systems, the formation of AFm phases provides an important intermediate CO_2-buffering capacity once portlandite is depleted. However, in low-kaolinite 2:1 activated-clay binders, where AFm formation is limited, carbonation is expected to progress more rapidly toward C-A-S-H decalcification, placing greater importance on the chemical stability of the gel itself.

The carbonation of low-Ca/Si C–S–H leads to the formation of amorphous silica gel, where the extent of shrinkage or densification depends on the Ca/Si ratio and the amount of bound water within the gel structure [17,27]. The loss of bound water during carbonation can trigger local shrinkage, resulting in pore coarsening instead of refinement [28]. In systems forming chemically distinct C-A-S-H with significant aluminum incorporation, such as those based on low-kaolinite 2:1 activated-clays, the resistance of the gel to decalcification and structural collapse is therefore expected to play a decisive role in governing carbonation damage.

Beyond changes in hydrate phase assemblage, carbonation drives dissolution–precipitation processes that modify microstructure and transport properties. In OPC systems, carbonation of CH commonly leads to pore refinement due to the larger molar volume of $CaCO_3$ [17,19,20]. However, carbonation of C–S–H follows a more complex decalcification–polymerization pathway that forms amorphous silica gel [5,20,29] and the resulting molar volume change depends strongly on the initial Ca/Si ratio, the water content of the silica gel, and the degree of hydration [30,31]. Consequently, carbonation can both refine or coarsen the microstructure depending on the initial Ca/Si ratio, water content in the silica gel, and the degree of hydration [17].

In addition to binder composition, the moisture state of the material is equally decisive in determining carbonation behavior, yet it is often overlooked. Even in the absence of CO_2, exposure to moderate relative humidity can significantly alter cement paste microstructure. Studies have shown that drying at 55–70% RH leads to gradual coarsening of the pore network due to collapse of fine pores, while the overall porosity remains relatively constant [32,33]. These microstructural changes influence transport properties [26,30,34,35] and therefore affect how carbonation proceeds. In binders with limited chemical buffering capacity, such as low-kaolinite clay-based systems, distinguishing between transport-driven pore structure changes induced by drying and chemical degradation driven by carbonation becomes particularly important.

Considering the global abundance of low-kaolinite clays, the limited durability data for these binders, and the critical role of carbonation in governing long-term performance, this study investigates how accelerated carbonation affects their fundamental properties. Specifically, we examine (i) changes in hydrate phase assemblage, (ii) the structure and chemistry of C-A-S-H, and (iii) the evolution of pore size distribution. To isolate chemically driven carbonation effects, drying-induced microstructural changes are explicitly decoupled from CO_2 exposure, and the influence of curing duration is assessed as a proxy for hydrate chemical maturity.

Building on our earlier work on the activation and hydration behavior of low-kaolinite 2:1 activated-clays [16,36], the present study examines how these binders respond to carbonation. The binder system used here was developed within our team, where Hazarika et al. investigated the activation and reaction mechanisms of locally sourced low-kaolinite clays subjected to a combined thermal-mechanochemical activation route, followed by a detailed assessment of their hydration behavior, strength development, and pore structure evolution. Together, these studies demonstrated that such clays can be effectively activated and used as SCMs despite their modest kaolinite content. Notably, the most recent work [16] showed that even at substitution levels up to 40%, these binders can achieve strengths comparable to OPC while forming pore structures broadly consistent with LC^3 systems. However, despite these encouraging mechanical and microstructural outcomes, the hydrate assemblage produced by low-kaolinite 2:1 activated-clays differs fundamentally from that of LC^3.

Carbonation in cementitious materials is commonly simulated under controlled laboratory conditions to accelerate the reaction and evaluate long-term behavior within a practical timeframe. The key parameters influencing the rate and extent of carbonation are relative humidity (RH), temperature, and CO_2 concentration, as these govern the rate of CO_2 diffusion and its reaction with hydration products. In addition to these exposure-related parameters, the chemical state of the hydrate assemblage at the time of exposure plays a decisive role, particularly in low-kaolinite activated-clay binders. An additional factor that plays a decisive role in low-kaolinite activated-clay binders is the curing duration prior to exposure, not simply because it increases the degree of hydration, but because it governs the chemical evolution of the hydrate phases, including the structure and aluminum incorporation within C-A-S-H. Although often overlooked, the time to exposure directly affects CO_2 uptake and reaction pathways, particularly in systems containing slow-reacting clays, where the composition and connectivity of C-A-S-H continue to evolve well beyond early ages, rather than remaining

chemically stable once formed. For consistency and simplicity, the present study adopts EN 12390–12:2020 [51], which prescribes 28 days of curing before carbonation exposure. However, in the case of low-kaolinite 2:1 activated-clays, such a curing duration may correspond to a chemically immature hydrate assemblage, in which aluminum incorporation and silicate polymerization in C-A-S-H are still developing. Given the prolonged hydration characteristic of low-kaolinite 2:1 activated-clays, this study explicitly examines the influence of extended curing on carbonation response, treating curing time as a parameter controlling hydrate chemistry and gel stability, rather than solely pore refinement or hydrate quantity.

To translate these research objectives into measurable outcomes, a multi-technique approach was adopted to study both chemical and microstructural changes during carbonation. X-ray diffraction (XRD) was used to identify the evolution of the hydrate phase assemblage, while thermo gravimetric analysis (TGA) provided quantitative insight into carbonate formation and portlandite consumption. ^{29}Si and ^{27}Al solid-state nuclear magnetic resonance (NMR) analyses were employed to examine changes in the C-A-S-H structure, including silicate polymerization and aluminum incorporation. Mercury intrusion porosimetry (MIP) was performed to assess the pore structure and its refinement or coarsening under both drying and carbonation conditions.

2. Materials and sample preparation methods

2.1. Materials

The materials used in this study are Ordinary Portland Cement (OPC), CEM I (52.5 R) supplied by Heidelberg Materials, and a clay sourced from Norrköping, Sweden. The chemical composition obtained from inductively coupled plasma atomic emission spectroscopy (ICP-AES) of OPC and raw clay is given in Table 1. The clay is a heterogeneous low-kaolinite clay composed primarily of illite (33%), smectite (28%), and kaolinite (21%), with mineralogical characterization additionally indicating the presence of interstratified illite-smectite mixed-layer phases. The raw clay exhibited a median particle size (D50) of approximately 50 μm. Following the combined thermal–mechanochemical activation route employed in this study, the activated-clay achieved a cumulative Modified R^3 heat release of approximately 350–355 J/g SCM, indicative of moderate pozzolanic reactivity. Further details regarding the activation procedure and physicochemical characterization are available in [36].

2.2. Activation of clay

In a previous study by our research group, various activation methods were investigated for the clay used in this work, and its reactivity was systematically evaluated [36]. Based on those findings, a combined thermal and mechanochemical activation approach was adopted in the present study. The clay was first thermally activated using a Nabertherm laboratory furnace. Approximately 500 g of raw clay was heated from ambient temperature to 800 °C and maintained at this temperature for 60 min.

Following thermal treatment, mechanochemical activation (MCA) was performed using a planetary ball mill (Retsch PM 100). Milling was carried out in a 500 mL grinding jar using 12 mm steel balls, with a ball-to-powder (B/P) mass ratio of 25. The milling process was conducted at a rotational speed of 500 rpm for 20 min.

2.3. Binder design

The primary blend investigated in this study incorporates 30% activated-clay as a replacement for OPC. Although previous study showed that replacement levels of up to 50% can achieve compressive strengths comparable to OPC [16], while forming pore structures broadly consistent with LC^3 systems. However, despite these encouraging mechanical and microstructural properties, the hydrate assemblage produced by low-kaolinite 2:1 activated-clay differs substantially from that of LC^3. Owing to their limited kaolinite content, these activated-clays supply less reactive aluminum, resulting in lower AFm formation. Instead, most of the aluminum becomes incorporated into the C-A-S-H gel. Consequently, the hydrate assemblage is characterized by reduced portlandite (CH), lower AFm CO_2 buffering capacity, and a chemically distinct C-A-S-H structure. Since carbonation resistance in blended systems is strongly influenced by the availability of calcium, particularly in the form of portlandite which acts as a primary buffer against CO_2 ingress, increasing levels of clinker substitution can significantly influence carbonation behavior. In activated-clay-blended binders, higher replacement levels reduce the amount of CH formed during hydration, while the reactive aluminosilicate phases of the activated-clay further consume CH through pozzolanic reactions. As a result, the overall calcium availability in the system progressively decreases with increasing activated-clay replacement. Therefore, to balance clinker substitution with sufficient calcium availability while capturing the distinctive hydrate chemistry of these binders, a binder containing 30% clay replacement (30C) was selected in the present study for carbonation investigation.

2.4. Casting of specimens and sample preparation for characterization

Mortars were cast in 50 mL tubes to study pore structure evolution and pastes were cast in 25 mL tubes for phase assemblage and C-S-H modifications. The binder-to-aggregate ratio was kept at 1:3, and the water-to-cement ratio was 0.50. The paste samples were rotated for 24 h after casting to minimize the risk of segregation between the binders and water. OPC samples were cured for 28 days, whereas activated-clay-blended binder was subjected to two curing regimes of 28 days (30C) and 100 days (30CLC) in order to investigate the effect of curing time on evolution of carbonation. The binder compositions and curing durations are summarized in Table 2. The schematic illustration for better understanding of sample preparation and conditioning is given in Fig. 1 for mortars and Fig. 2 for pastes. After curing the samples were cut into 4 equal sections (height 2 cm). The samples were coated with epoxy on all sides, except top to ensure unidirectional carbonation and drying. The samples were then subjected to pre-treatment conditioning at a temperature of (20 ± 2)°C and a relative humidity of (57 ± 3)% for 14 days. Following this, the samples were exposed to carbon dioxide in a carbonation chamber with a carbon dioxide concentration of (3.0 ± 0.5)%, also maintained at (20 ± 2)°C temperature and (57 ± 3)%

Table 2
Binder composition and curing durations.

Sample Designation	SCM	Curing
OPC	–	28 days
30C	30% Activated-clay	28 days
30CLC	30% Activated-clay	100 days

Table 1
Chemical composition of ordinary Portland cement and raw clay.

wt%	SiO_2	Al_2O_3	Fe_2O_3	CaO	MgO	Na_2O	K_2O	TiO_2	SO_3	MnO	P_2O_5	SrO	BaO	LOI	Total
OPC	19.60	4.50	3.00	62.20	3.50	0.27	1.01	–	3.50	–	–	–	–	2.50	100.08
C	51.80	18.35	9.55	1.32	3.34	1.70	4.42	0.87	–	0.11	0.15	0.01	0.08	8.15	99.86

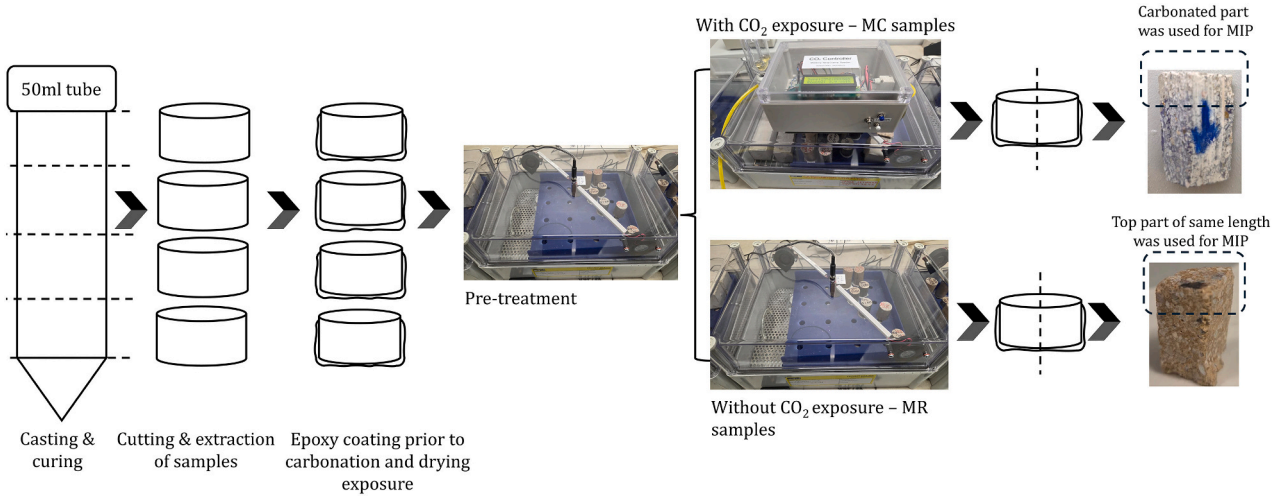

Fig. 1. Schematic illustration of the mortar sample preparation, and conditioning.

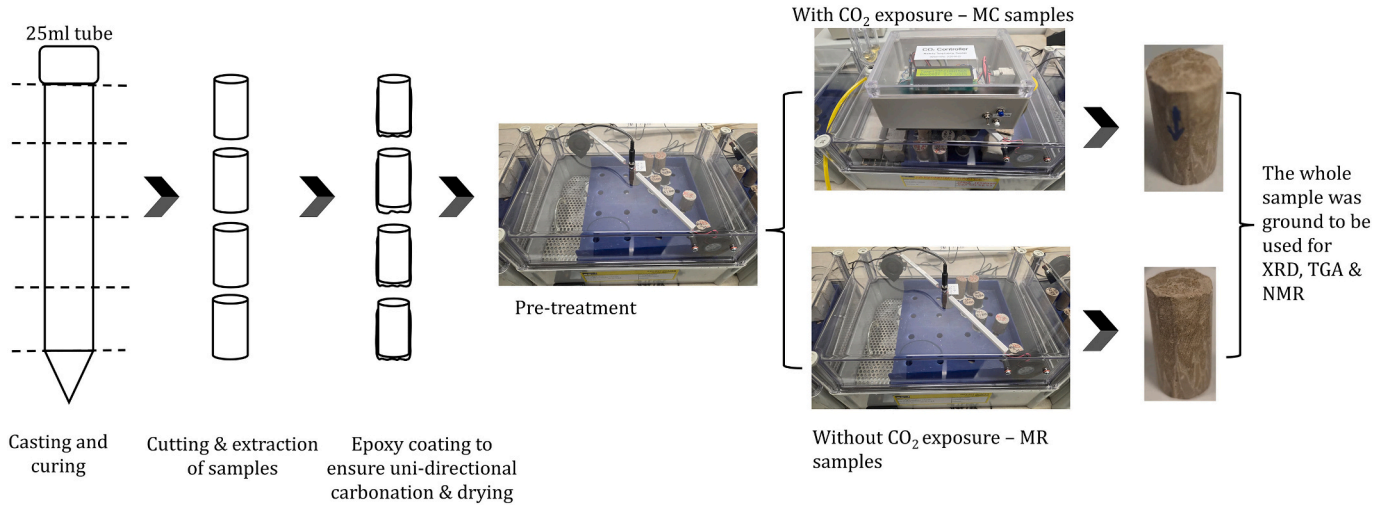

Fig. 2. Schematic illustration of the paste sample preparation, and conditioning.

relative humidity, in accordance with EN 12390–12:2020 [37]. To decouple drying effects from carbonation, companion samples of each mix were kept under identical temperature and relative humidity conditions i.e. (20 ± 2) °C and (57 ± 3) % RH without CO_2 exposure. Sample designations are defined as follows: MR refers to month-dried reference samples, MC refers to month-carbonated samples.

Table 3 gives conditioning details of samples under pre-treatment, drying and carbonation.

The planned carbonation durations were 1, 2, 4, and 6 months. At each interval, samples were removed from the carbonation chamber. Mortar specimens were then saw-cut into pieces of approximately 1 × 2 cm (for OPC and 30C), 1 × 3 cm (for 30CLC) and phenolphthalein pH indicator were sprayed onto the freshly cut surfaces to distinguish between carbonated and uncarbonated regions. The carbonated portions were subsequently separated and used for further analysis. Details of the carbonation depth measurements are provided in supplementary material S1. Companion samples subjected only to drying were taken at the same durations. Following this, the samples underwent a combined solvent exchange and vacuum oven drying procedure. The samples were immersed in isopropanol for 5 days, with the solvent replaced daily to ensure complete water removal. Subsequently, the samples were dried in vacuum oven at 30 °C for 2 days. Once these steps were completed, the samples were prepared for specific pore structure analysis, C-S-H structure evolution and hydrate phase assemblage experiments. For Nuclear Magnetic Resonance (NMR), Thermogravimetric Analysis (TGA) and X-ray Diffraction (XRD), the paste samples (whole 2 cm piece as shown in Fig. 2) are manually ground in a mortal and then sieved to achieve a particle size of less than 75 μm. For Mercury Intrusion Porosimetry (MIP), specimens were extracted from the top (carbonated) region, as shown in Fig. 1. For drying-only samples, material was taken from the same depth to ensure comparability and isolate the effect of carbonation. The samples were then crushed into fragments of 2–8 mm for MIP testing. MIP measurements were performed on duplicate specimens, and the reported values represent the average of two measurements.

Exposure to atmospheric CO_2 during sample preparation cannot be completely avoided; however, all samples were handled under identical conditions and stored in a vacuum desiccator containing silica gel to

Table 3
Conditioning of samples.

Condition	Pre-treatment (for MR & MC)	Drying (MR samples)	Carbonation (MC samples)
All samples (OPC, 30C, 30CLC)	20 ± 2)°C & (57 ± 3)% RH	(20 ± 2)°C & (57 ± 3)% RH	(20 ± 2)°C, (57 ± 3)% RH & 3% CO_2

minimize moisture ingress and ensure consistency in the comparative analysis.

The raw data for undried, uncarbonated samples were taken from [16], and are used here solely as a reference for hydrate phase assemblage and C-A-S-H evolution under hydration conditions. That study focused exclusively on hydration behavior and did not include drying or carbonation. In [16], OPC and 30C samples were cured for 28 days, while 30CLC samples were monitored up to 56 days, which represents the latest reported hydration state for this system prior to any subsequent conditioning.

In the present study, 30CLC specimens used for carbonation experiments were cured for 100 days to account for the slower pozzolanic reactivity of low-kaolinite 2:1 activated-clay. While hydration data beyond 56 days are not available from [16], the 56-day state is considered representative of a late-age hydrate assemblage, as that study showed continued but gradual hydrate evolution beyond early ages, without abrupt changes in phase identity. Accordingly, the 56-day data are used here as a baseline reference for the chemically matured, uncarbonated system, against which carbonation-induced changes are assessed.

3. Characterization methods

3.1. X-ray diffraction

XRD was conducted on carbonated as well as uncarbonated pastes, to study the effect of carbonation on hydrate phase assemblage of OPC and 30C blends. Bruker D8 Discover was used with 2 theta ranges 5^{o} - 60^{o} with step size 0.02^{o}, time per step 0.8 s. To identify the phases DIFFRAC. EVA V5.2 software was used. XRD was employed for phase identification and qualitative tracking of phase evolution. Quantitative phase analysis (e.g., Rietveld refinement) was not performed, as quantitative assessment was primarily obtained from thermogravimetric analysis (TGA).

3.2. Thermogravimetric analysis

Thermogravimetric analyses were performed on a Mettler Toledo TGA/DSC 3+ under nitrogen purge (flow 50 mL min^{-1}). Approximately 8–10 mg of powdered sample was loaded into alumina pans and heated from 20 to 1000 °C at a constant heating rate of 10 K min^{-1}. Using STARe v20 mass losses were evaluated over 40–520 °C (hydrate water), 400–500 °C (CH), and 520–820 °C ($CaCO_3$). CH and $CaCO_3$ contents were calculated from respective mass losses using stoichiometric factors and expressed as % weight relative to the mass at 520 °C.

Thermogravimetric analysis (TGA) data of cementitious materials often exhibit overlapping mass-loss events due to the simultaneous decomposition of multiple hydrated phases within similar temperature ranges. To resolve these contributions, a deconvolution of the derivative thermogravimetric (DTG) curves was performed using the OriginPro® 2023 peak analyzer. The experimental DTG signal was fitted as a sum of individual peaks, each corresponding to a distinct thermal event, enabling separation and quantification of the contributions of especially ettringite and AFm phases, which were otherwise difficult to distinguish due to their overlapping decomposition behavior. For the deconvolution, Gaussian peak functions were employed to simplify the fitting procedure and to ensure a consistent representation of the overlapping processes. Prior to peak fitting, the derivative curve was corrected using a straight-line reference over the selected temperature range. The amounts of ettringite and AFm were quantified by integrating the area under the corresponding mass-loss peaks; a representative example of the deconvolution procedure is provided in the Supplementary material S2. Ettringite was evaluated using the center-of-gravity region between 80 and 90 °C, while AFm was quantified from the 110–140 °C and 230–260 °C interval. In the clay-blended systems, monocarbonate is the predominant AFm phase with a minor contribution from hemicarboaluminate, as indicated by XRD. Due to overlapping decomposition ranges, AFm phases cannot be distinguished by TGA and are therefore reported collectively.

Unless stated otherwise, all characterization results reported in this study correspond to single measurements. Repeat analyses were not performed due to the comparative nature of the work and the large experimental matrix investigated, with emphasis placed on relative trends rather than absolute values. For reference, a previous study has reported a standard deviation of approximately 0.2 wt% for CH determination based on thermogravimetric analysis on triplicate measurements using a comparable methodology [38].

3.3. ^{29}Si and ^{27}Al nuclear magnetic resonance (NMR)

The modifications in C-S-H structure due to carbonation were studied by magic angle spinning (MAS) Nuclear Magnetic Resonance (NMR). All ^{29}Si and ^{27}Al MAS NMR experiments were conducted at 298 K using a Bruker 4 mm MAS BB/1H probe. Powdered samples (~0.09–0.12 g) were packed into 4 mm zirconia rotors for analysis. The ^{29}Si MAS NMR spectra was acquired using high-powered proton decoupling (HPDEC) with a spinning rate of 7.5 kHz. A total of 2500 scans were accumulated using a 3 μs pulse (~45° flip angle) and a relaxation delay of 30 s. The 27Al HPDEC MAS NMR spectra was obtained at a spinning rate of 11 kHz with 2048 scans, using a 4 μs pulse (~65° flip angle) and a relaxation delay of 0.8 s. For both nuclei SPINAL64 proton decoupling was employed with a 1H-field strength of 50 kHz [39].

Peak deconvolution was performed using the Interactive Peak Fitting (IPF) software, version 13.2.0.0 [40], which operates within the MATLAB environment (version 2024b). A combination of Lorentzian and Gaussian functions was used for curve fitting. The software automatically determined the optimal mixing ratio between the two profiles during the fitting process based on the number of peaks manually selected by the user. The relative intensities of Q^n species and structural characteristics of C-S-H phase were evaluated from the deconvoluted ^{29}Si MAS NMR spectra. The structural parameters of C-S-H average chain length (CL), silicate chain length (CL_Si) and Al/Si molar ratio for Al are incorporated into silicate chains of the C-S-H structure using following equations adapted from [41].

$$CL = \frac{2\left[Q^1 + Q^2 + \frac{3}{2}Q^2(1Al)\right]}{Q^1} \tag{1}$$

$$CL\_Si = \frac{2\left[Q^1 + Q^2 + Q^2(1Al)\right]}{Q^1 + Q^2(1Al)} \tag{2}$$

$$\frac{Al}{Si} = \frac{Q^2(1Al)}{2\left[Q^1 + Q^2(1Al) + Q^2\right]} \tag{3}$$

The level of decalcification (L_d) was evaluated by comparing the relative intensities related to C-S-H (Q_b^n and Q_a^n) before and after carbonation respectively using the following equation and is given in Fig. 7(e) [42]:

$$L_d = \left(1 - \frac{Q_a^1 + Q_a^2}{Q_b^1 + Q_b^2}\right) x\ 100 \tag{4}$$

Semi quantitative degree of silicate polymerization is simply calculated by using the following equation adopted from [42] and is given in Fig. 7(f).

$$\frac{B}{A} = \left(\frac{Q^3 + Q^4}{Q^1 + Q^2}\right) \tag{5}$$

3.4. Mercury intrusion porosimetry

Mercury intrusion porosimetry was performed using a Micromeritics AutoPore V 9620 instrument. The instrument is capable of applying

pressures in the range of 0.001–414 MPa, corresponding to a calculated pore diameter range of approximately 0.003–800 μm. The pore diameter was calculated using the Washburn equation.

$$r = -\frac{2\gamma cos\theta}{P} \quad (6)$$

where r is the pore radius, γ is the surface tension of mercury (0.485 $N{\cdot}m^{-1}$), θ is the contact angle (130°), and P is the applied pressure. The calculation assumes cylindrical pore geometry and non-wetting conditions, meaning that smaller pores require higher intrusion pressures. High-resolution data were collected with intrusion and extrusion volume precision better than 0.1 μL.

4. Results and discussion

The following sections present and discuss the results in relation to the research objectives, aiming to provide a coherent and logically structured interpretation of the findings.

4.1. Effect of carbonation on hydrate phase assemblage

The combined XRD-TGA analysis provides insight into how carbonation alters the hydrate phase assemblage. XRD patterns of OPC, 30C, and 30CLC pastes are shown in Fig. 3(a, b & c). For each system, samples carbonated for 1, 2, 4, and 6 months are included alongside their respective uncarbonated reference samples at equivalent ages. Fig. 4 illustrates the complementary TGA based quantification of CH (Fig. 4a), hydrate water (Fig. 4b), and calcite contents (Fig. 4c) in OPC, 30C, and 30CLC pastes, comparing undried, reference (MR), and carbonated (MC) samples. In addition, Fig. 5(a) illustrates how ettringite evolves under carbonation, whereas Fig. 5(b) depicts the corresponding evolution of AFm.

4.1.1. Hydrate phase assemblage prior to carbonation

In Undried hydrated state OPC, 30C and 30CLC the major crystalline phases identified include portlandite (CH) at 2θ 18°, 28.6° and 34° [43,44], corresponding to the (001) and (002) crystallographic planes, respectively. Ettringite (E) appeared at 2θ 9.1° [43] and Afm phases were identified at 2θ 11.2° - 11.6° [43]. These peak positions confirm the presence of CH, AFt, and AFm in all three systems, and are consistent with hydrate assemblages reported for OPC [45] and LC^3 binders [3,46,47]. In the previous study on hydration of the same 2:1 mixed-layer activated-clay systems, the AFm assemblage is expected to be dominated by carbonate-bearing phases (hemicarboaluminate and monocarbonate), rather than monosulfoaluminate, owing to the availability of carbonate and the relatively slower release of aluminate species [16].

TGA provides complementary quantitative information about the phase assemblage. In undried hydrated state, OPC showed highest portlandite content in comparison to 30C and 30CLC [48]. This reduced portlandite content in activated-clay blended binders is attributed mainly to two factors. First, the dilution effect reduces the absolute amount of clinker in these blended systems, limiting the potential for portlandite formation. Second, the activated mixed-layer clay exhibits significant pozzolanic reactivity, the reactive aluminosilicates consume CH as they react to form additional C-A-S-H gels [5,49]. The CH contents of 30C and 30CLC are very similar, with only a slightly higher CH content observed in 30C. This small reduction in CH for 30CLC can be attributed to continued, but limited, pozzolanic reaction during the extended curing period, resulting in minor additional consumption of portlandite [36,50]. This indicates that the majority of the pozzolanic reaction is already completed by 28 days of curing, such that prolonged curing does not lead to substantial further reductions in CH content.

As noted in previous studies, activated 2:1 layered aluminosilicates such as smectite and illite react with water and portlandite to form additional C-A-S-H with a lower Ca/Si ratio [20,51,52]. Although these activated-clays exhibit slower pozzolanic kinetics than kaolinite [4,53], their reactivity persists over time. Consequently, extended curing in 30CLC primarily enhances the degree of hydration and promotes continued hydrate evolution and microstructural refinement, rather than significant additional CH consumption. The reduced formation of AFm phases is therefore attributed to the preferential incorporation of Al into the C-A-S-H gel during ongoing hydration [16].

Hydrate water also varies among the systems, reflecting differences in their degree of hydration and enabling direct comparison between the binders. OPC exhibits the highest bound water, consistent with its higher degree of hydration. The 30C binder shows lower hydrate water, reflecting the limited hydration achievable after 28 days, whereas 30CLC contains a higher hydrate water content than 30C, approaching that of OPC and demonstrating the influence of prolonged curing.

The deconvoluted DTG signals reveal clear differences in aluminate hydrate distribution among the three systems. The largest ettringite (AFt) peak area is observed in 30C, consistent with active early-age aluminate hydrate formation. In contrast, 30CLC exhibits the highest AFm peak area, reflecting the expected progression of hydration due to prolonged curing, where part of the AFt has converted to AFm and additional aluminum has been incorporated into the C-A-S-H gel. OPC shows intermediate amounts of both AFt and AFm. These distinctions highlight how curing duration and pozzolanic reactions govern the evolution of aluminate hydrates even prior to drying or carbonation.

4.1.2. Effect of drying de-coupled from carbonation on hydrate phase assemblage

In the dried state, the XRD patterns of OPC, 30C, and 30CLC show that the characteristic reflections of the main hydrate phases including portlandite (CH), ettringite (AFt), and AFm appear at the same 2θ positions as in the undried samples. Drying does not introduce any new crystalline phases, indicating that the primary hydration products formed under sealed curing conditions remain stable and structurally preserved. Consistent with this observation, TGA analysis shows no measurable change in CH content upon drying, confirming that portlandite is not significantly affected by exposure to 20 °C and 57% RH. When exposed to drying, a slight reduction in hydrate water is observed at 1MR across all binders. This initial decrease is attributed to the removal of physically bound and weakly held gel water. It is well established that when the relative humidity drops below approximately 75–80%, hydration reactions effectively halt, limiting further bound-water development and influencing the measurable degree of hydration [33]. Beyond 1MR, the hydrate water content remains relatively stable at 2MR, 4MR, and 6MR, indicating that the remaining bound water is structurally incorporated within the C-A-S-H and other hydrates and is therefore less sensitive to drying at the applied relative humidity.

4.1.3. Effect of carbonation coupled with drying on hydrate phase assemblage

Carbonation of OPC pastes leads to significant changes in the mineralogical composition, as reflected in the XRD patterns of the MC samples (Fig. 3a). In carbonated OPC the main type of carbonation product formed is calcite at $2\Theta = 29.4^{o}$. Upon exposure to carbon dioxide for 1 to 6 months the Fig. 3(a), gradual calcite formation and CH depletion particularly in 4MC and 6MC can be observed. Although calcite is the major representative peak, weak shoulders or broad peaks appear in the 2θ range of 26.6° to 27.2°, which can be attributed to the formation of vaterite (110) and aragonite (111,021) [54] in 4MC and 6MC samples suggesting that prolonged exposure to CO_2 is facilitating the formation of polymorphs of calcite. Calcium carbonate is the principal reaction product of carbonation which can precipitate in three calcite polymorphs including calcite, aragonite and vaterite. Among these calcite is the most stable one whereas aragonite and vaterite are metastable phases that may gradually transform into calcite over time [20].

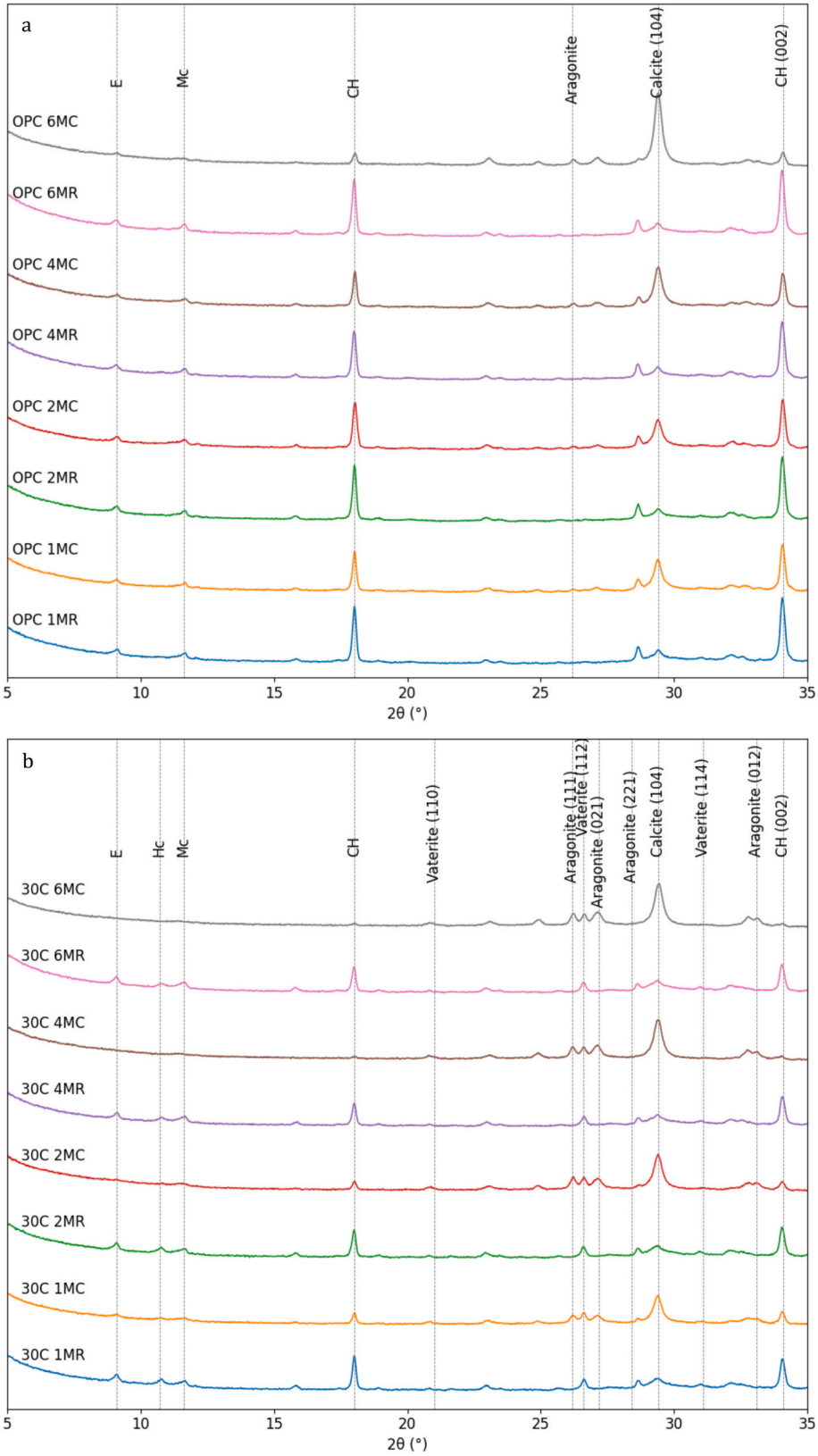

Fig. 3. XRD hydrate phase evolution under carbonation and drying over one four and six months (a) OPC, (b) 30C, & (c) 30CLC. Panel (c) is presented on the following page.

In comparison with OPC, the blended binder 30C exhibits a modified carbonation behavior as shown in Fig. 3b, majorly because of lower initial CH content available and pozzolanic activity of activated-clay. The primary CH peak at $2\Theta = 18^{o}$ progressively becomes less intense

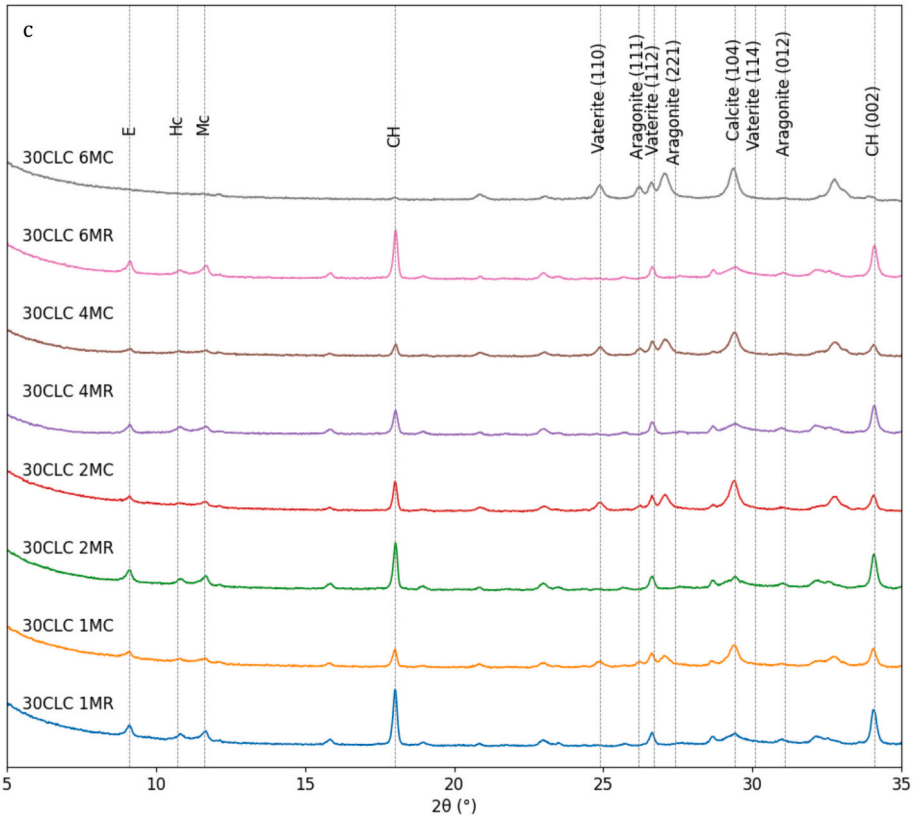

Fig. 3. (*continued*).

with carbonation exposure from 1 to 6 months. The major calcite peak appears at $2\Theta = 29.4^{o,}$ also secondary peaks emerge in the 24–30° 2θ range, which can be attributed to the formation of vaterite (e.g., 24.9° & 27.2°) and aragonite (e.g., 26.2° & 33.1°) simultaneously. Similar to 30C, carbonation exposure of 30CLC (Fig. 3c) leads to a substantial attenuation of the portlandite (CH) reflections at 2θ 18.0° and 34.1°, with these peaks becoming barely distinguishable by 4MC and nearly absent at 6MC. On the other hand, in the case of OPC, CH peak is still visible even in 6-month carbonated sample. In addition to that, besides calcite 30CLC shows more prominent aragonite and vaterite peaks.

In case of 30C CH peak is nearly disappeared by 4 months of carbonation, indicating rapid portlandite consumption. This behavior is attributed to lesser initial CH, insufficient hydration, a rather coarse pore structure which facilitated CO_2 ingress and accelerated carbonation. In contrast the 30CLC system retained CH at 4 months. In the 30C and 30CLC systems, ettringite disappears after six months of carbonation, coinciding with the complete consumption of portlandite (CH). This simultaneous loss indicates that the pore solution pH has dropped below approximately 10, the threshold at which ettringite becomes unstable and decomposes under these conditions [20,55].

TGA results corroborate the XRD results and show the evolution of portlandite (CH) content during carbonation in the two binder systems investigated (Fig. 4a). While CH consumption is observed in both systems, the carbonation kinetics differ substantially. In OPC, a significant reduction in CH is evident at 1MC; however, CH levels remain comparatively stable between 1MC and 4MC, indicating a sustained buffering capacity against carbonation. A further decrease in CH content is observed at 6MC. In contrast, the activated-clay binder exhibits a more progressive and continuous reduction in CH with increasing carbonation duration. CH depletion occurs earlier in 30C, whereas prolonged curing in 30CLC delays, but does not prevent CH consumption, with complete depletion observed by 4MC in 30C and by 6MC in 30CLC. The earlier loss of CH in the activated-clay systems results in a more rapid decline in pore solution alkalinity, thereby promoting earlier destabilisation of AFt and AFm phases and advancing C-A-S-H decalcification relative to OPC.

With carbonation (1MC to 6MC), a gradual decrease in hydrate water (Fig. 4b) was observed in all binders. This reduction results from the decalcification and destabilisation of hydrates during carbonation, where bound water is released as hydrates convert into carbonate phases. The decrease was more pronounced in the activated-clay systems, particularly 30C, which had lower overall hydrate stability compared to OPC. Part of this water loss can also be attributed to the decomposition of ettringite, which becomes unstable under the lower pH conditions associated with carbonation.

The evolution of ettringite and AFm after six months of carbonation exposure is quantified in Fig. 5a, and Fig. 5b, respectively. After six months of carbonation (6MC), however, both AFt and AFm decrease sharply in all systems. In 30C and 30CLC, ettringite is almost completely consumed, and AFm is reduced to a minor fraction of its original quantity. The XRD patterns show that AFt reflections disappear almost entirely in these binders, and only OPC retains a faint ettringite signal after prolonged exposure. These observations are consistent with the known carbonation pathways of sulfoaluminate hydrates: ettringite carbonates to aragonite and an amorphous alumina–silica gel, AFm phases decalcify to calcite with an alumina-rich residue, and carbonation of C-A-S-H produces a mixture of aragonite and vaterite [56]. Accordingly, the emergence and intensification of aragonite and vaterite peaks in the 4MC and 6MC XRD patterns of the activated-clay-blended binders reflect the progressive decomposition of AFt and AFm and the onset of C-A-S-H carbonation. The extent to which these phases decompose differs markedly between OPC and the activated-clay binders. The much stronger depletion of AFt and AFm in 30C and 30CLC can be attributed to their lower initial CH content, which limits their pH-buffering capacity during carbonation. As CH is consumed earlier in these systems, the pore solution pH drops more rapidly, accelerating the destabilisation of sulfoaluminate hydrates and exposing

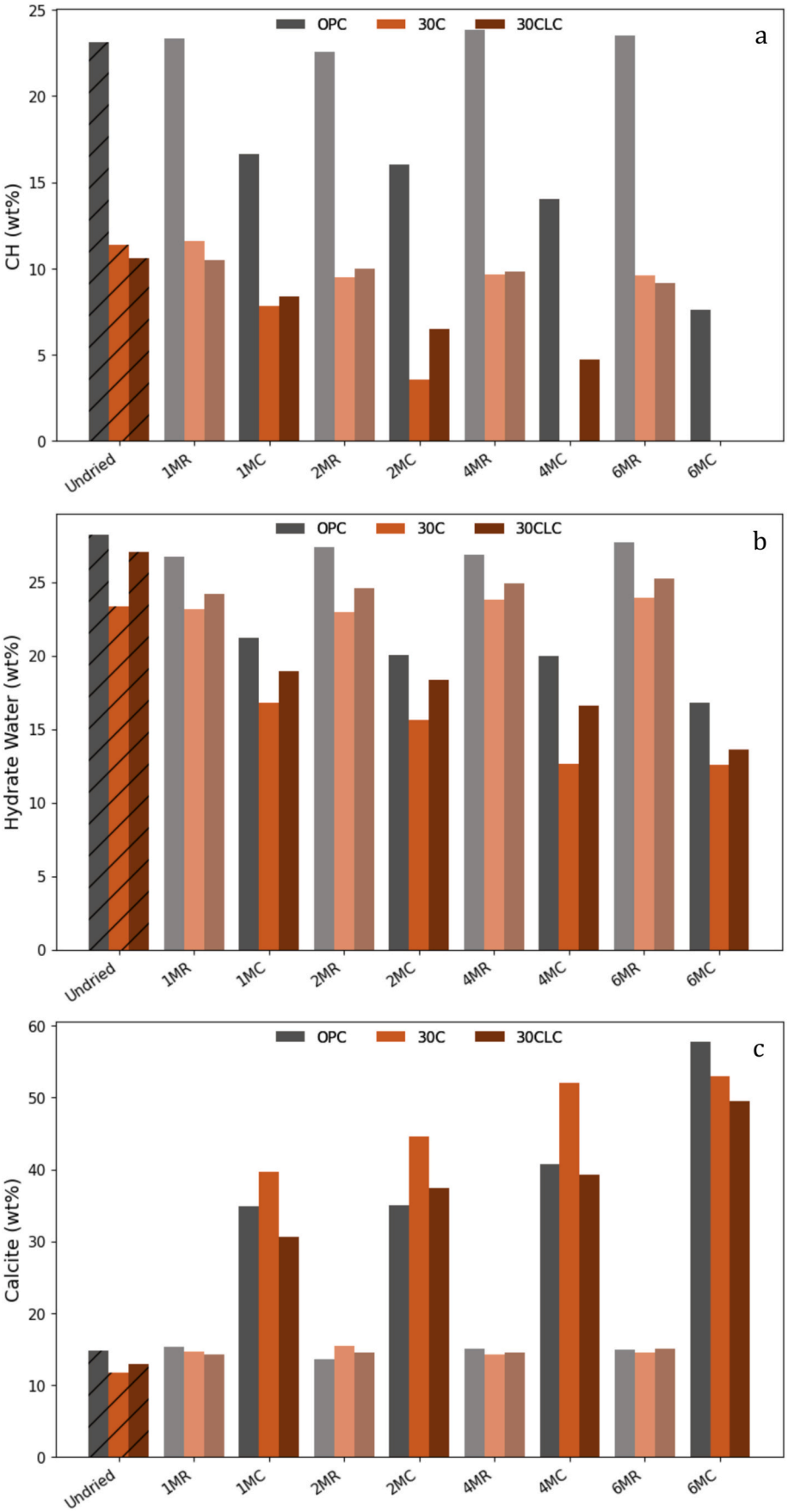

Fig. 4. TGA of Uncarbonated and carbonated OPC, 30C and 30CLC. (a) % CH, (b)% Hydrate water & (c)% Calcite.

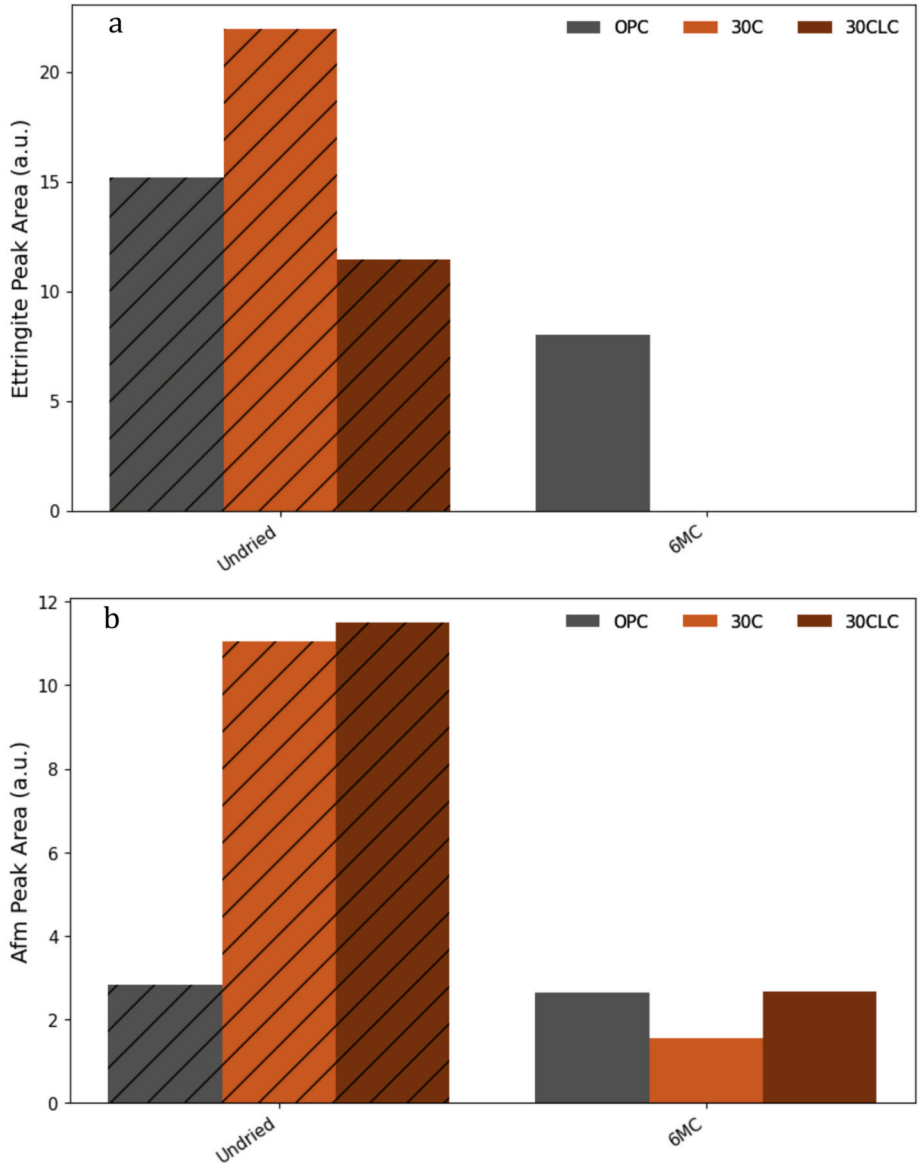

Fig. 5. TGA of Undried and carbonated OPC, 30C and 30CLC. (a) Ettringite & (b) AFm.

C-A-S-H to carbonation sooner than in OPC. However, following the carbonation sequence described in RILEM TC 281-CCC, AFm and AFt carbonate after CH but before deep C–S–H decalcification [20]. Thus, the higher initial AFm and AFt contents in the activated-clay binders especially in the more matured 30CLC system provide an intermediate carbonation "sink," allowing these phases to react first and thereby delaying the onset of aggressive C-A-S-H decalcification. This mechanistic CO_2 buffering effect is consistent with the NMR results presented in the next section, where earlier signatures of Si and Al polymerization appear in 30C than in 30CLC, indicating that the richer sulfoaluminate content in 30CLC affords temporary protection to the C-A-S-H gel during the early stages of carbonation.

In both binder systems, calcite formation shows an increasing trend with carbonation ages (Fig. 4c). At 1, 2, and 4 months of carbonation, calcite formation in 30C is consistently higher than in both OPC and 30CLC. In contrast, 30CLC exhibits the lowest calcite content across almost all ages, which can be attributed to its denser pore structure and the reduced availability of CH for carbonation. By 6 months, however, OPC shows the highest calcite formation, reflecting its greater CO_2 uptake capacity at later ages due to the initially higher CH availability.

4.2. Carbonation induced structural modifications of C–A-S–H

The structural modification of C-A-S-H was investigated using ^{29}Si MAS NMR spectra of OPC, 30C and 30CLC are shown in Fig. 6 (a, b & c). To facilitate interpretation of the spectral changes, key structural parameters of the C–S–H were quantified, including the chain length (Fig. 7b), silicate chain length (SiCL; Fig. 7d) and Al/Si molar ratio (Fig. 7c), which reflects the degree of Al incorporation into the silicate chains of the C–S–H structure. The degree of decalcification (L_d) is presented in Fig. 7(e), while a semi-quantitative evaluation of silicate polymerization, expressed as the bridging-to-paired tetrahedra ratio (B/A), is shown in Fig. 7(f).

4.2.1. C-A-S-H structure prior to carbonation stage

In the undried OPC sample (Fig. 6a), the dominant resonance at −78.5 ppm corresponds to Q^1, representing silicon atoms in the C–S–H chain-end sites [58], while the shoulder around −84.5 ppm corresponds to Q^2, associated with chain-middle groups [59]. A resonance centered at −81.5 ppm is attributed to $Q^2(1Al)$, reflecting partial substitution of Si by Al in the silicate framework [60]. The relative Q^n intensities are given in Fig. 7(a). For both 30C (Fig. 6b) and 30CLC (Fig. 6c) binders, Q^1

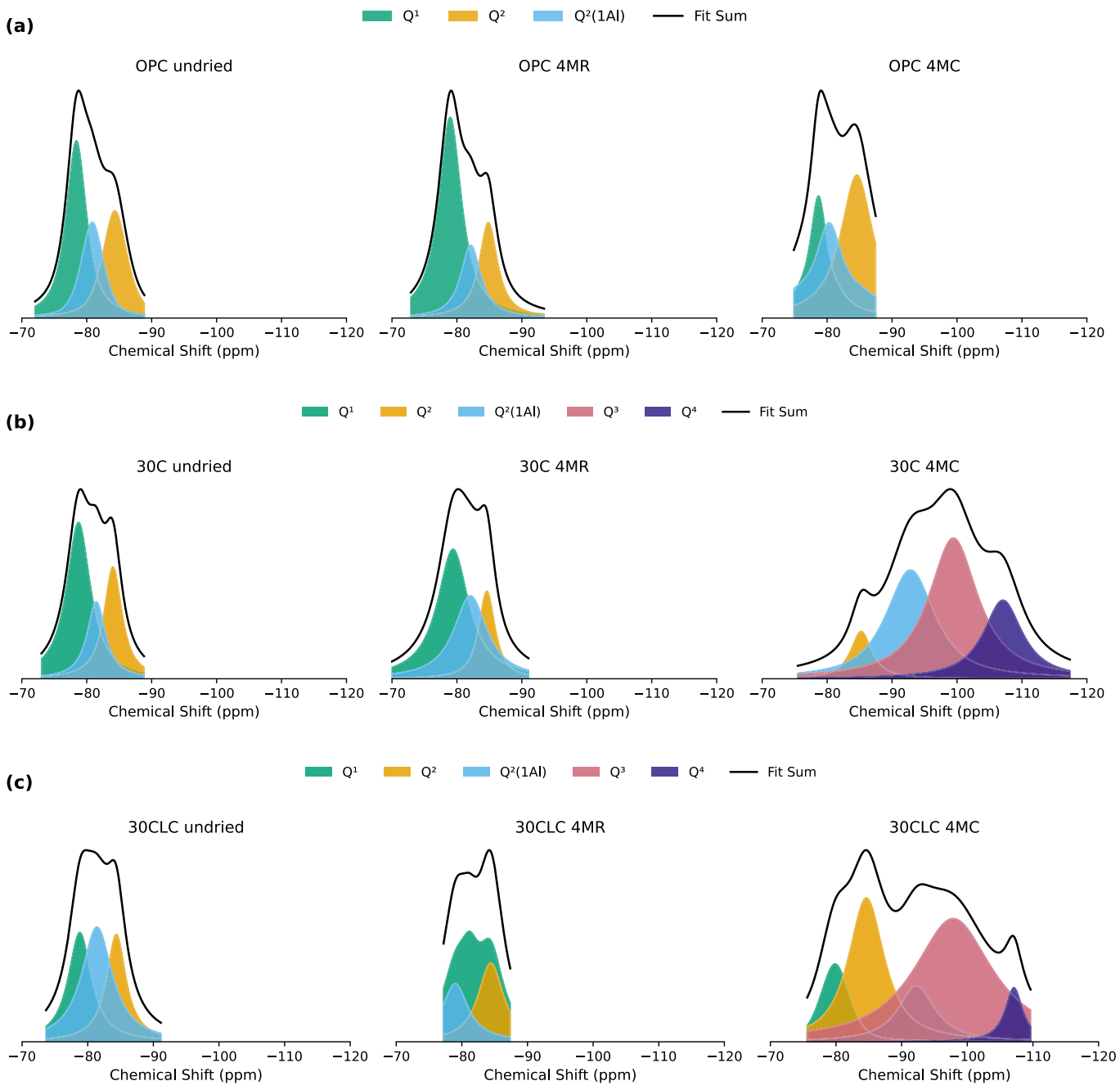

Fig. 6. ^{29}Si MAS NMR (a) OPC undried, uncarbonated and carbonated samples (b) 30C undried, uncarbonated and carbonated samples (c) 30CLC undried, uncarbonated and carbonated samples.

appears near −78.7 ppm, Q^2 between −84.0 and − 84.4 ppm, and Q^2(1Al) around −81.5 ppm. However, notable differences in peak intensities indicate changes in the relative abundance of local silicate environments within the C–(A)–S–H structure. The 30C sample, cured for 28 days, displays a Q^1/Q^2(1Al) distribution similar to OPC, suggesting a C-A-S-H structure with limited early Al incorporation. In contrast, the 30CLC system, with prolonged curing, exhibits reduced Q^1 intensity and a marked increase in Q^2(1Al), indicating enhanced substitution of Si by Al and greater silicate chain connectivity. These observations suggest that extended curing promotes further development and polymerization of the C-A-S-H gel network in the presence of low-reactivity activated-clay. C-A-S-H at zero carbonation stage. At zero carbonation stage, for the undried samples, distinct differences in the C-A-S-H nanostructure are observed between OPC, 30C, and 30CLC. OPC-Undried exhibits a chain length (CL ≈ 4.4), silicate chain length (SiCL ≈ 2.7), and a low Al/Si ratio (≈ 0.12), characteristic of Ca-rich C–S–H with limited silicate polymerization and minimal Al incorporation. Notably, CL values for OPC-Undried and 30C-Undried are essentially identical, indicating that 28 days of curing is insufficient for the activated-clay system to significantly modify the C–S–H chain structure. This suggests that pozzolanic reaction and Al incorporation in 30C are still limited at this early age. In contrast, 30CLC-Undried shows a markedly higher CL (≈ 7.9), nearly double that of OPC, together with the highest Al/Si ratio (≈ 0.21). This indicates substantially enhanced Al incorporation into the silicate chains and the formation of a more polymerized C-A-S-H structure, attributable to prolonged curing and sustained pozzolanic reaction. Despite these differences in chain length and Al substitution, the SiCL values remain similar across all three systems,

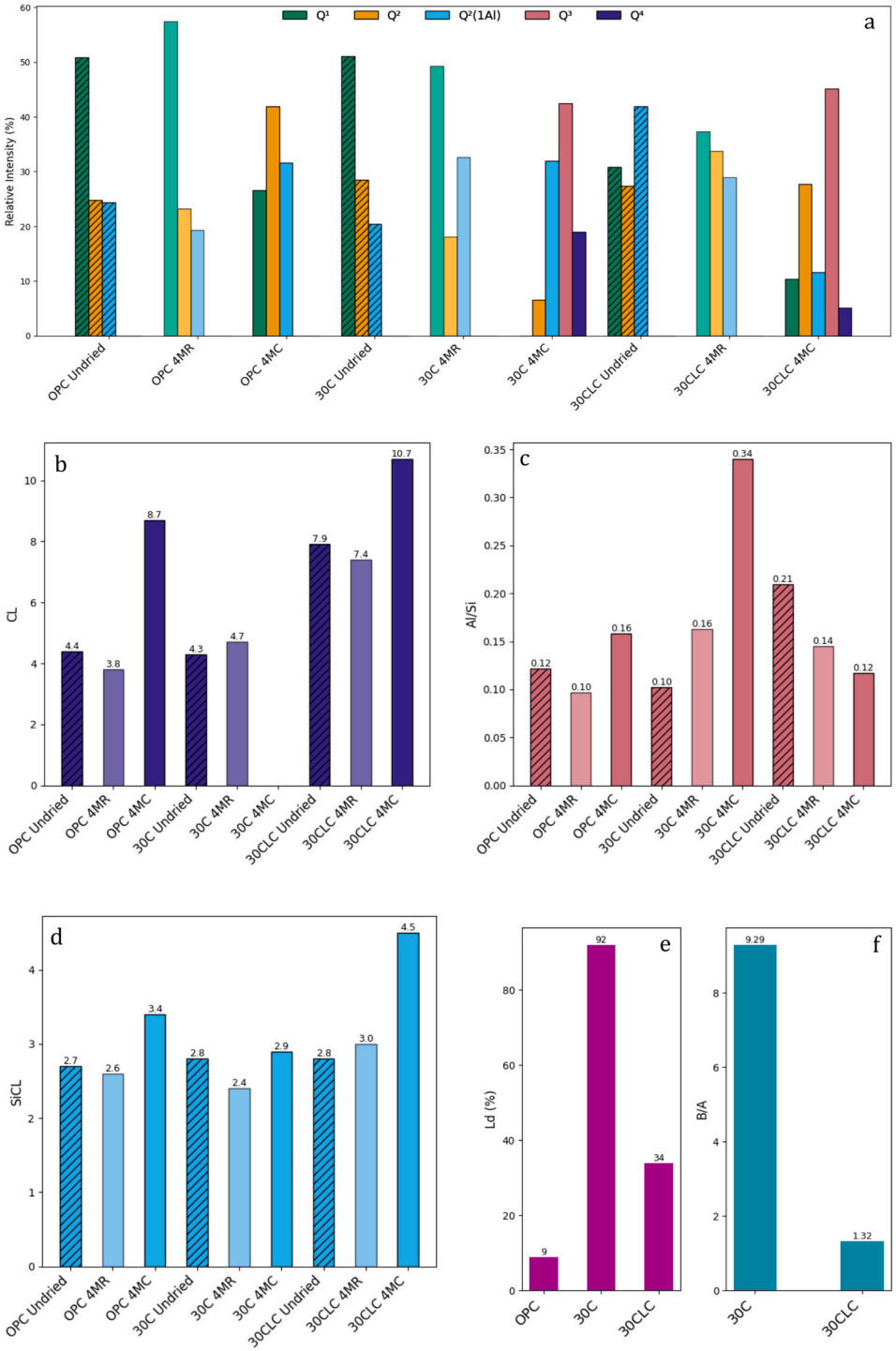

Fig. 7. (a) Q^n intensities, (b) chain lengths, (c) Al/Si Ratios, (d) silicate chain lengths, (e) level of decalcification & (f) B/A.

suggesting that the primary structural distinction arises from Al incorporation and chain extension rather than changes in silicate chain topology.

4.2.2. Effect of drying de-coupled from carbonation on C-A-S-H

Upon transitioning from the undried to the 4MR (dried) condition, the influence of drying becomes evident and appears to vary depending on the system as shown in Fig. 7 and Fig. 6. In OPC, drying results in a clear increase in Q^1 intensity (from 51% to 57%) alongside a reduction in both Q^2 and Q^2(1Al) components. This shift is indicative of partial depolymerization of silicate chains, possibly due to drying-induced reorganization. In the 30C system, the changes are more modest as Q^1 slightly increases while Q^2 decreases, yet the Q^2(1Al) contribution remains relatively stable. This suggests that Al substitution within the silicate network is retained even after drying. Interestingly, in the 30CLC system, drying leads to an increase in Q^1 and a corresponding decrease in Q^2(1Al). This evolution may reflect a more polymerized and stable C-A-S-H structure, likely resulting from the extended curing duration compared to the 30C sample. These observations suggest that longer curing enhances structural development and mitigates drying induced depolymerization, particularly in activated-clay-containing binders.

4.2.3. Effect of carbonation coupled with drying on hydrate phase assemblage

In the carbonated OPC sample, the Q^1 peak is significantly reduced in intensity, while the sharp Q^2 peak observed in the uncarbonated state becomes noticeably broader upon carbonation. In 30C the Q^1 peak completely disappeared after carbonation indicating the polymerization of silicate chains and transformations of C-S-H into more polymerized structure. However, in case of 30CLC Q^1 is retained even after 4 months of carbonation exposure, which means that longer curing has been proven beneficial in providing resistance to carbonation.

In the carbonated 30C and 30CLC samples, two new resonances emerge at −93.4 ppm and − 103.0 ppm for 30C, and at −93.5 ppm and − 102.5 ppm for 30CLC, corresponding to Q^3 and Q^4 environments, respectively [58]. The appearance of these Q^3 and Q^4 resonances indicates the formation of more highly polymerized silicate structures during carbonation. Q^3 species reflect silicate units with three bridging oxygens, while Q^4 species represent fully polymerized silica networks.

To provide an integrated perspective, and to enhance interpretation these spectral changes, we evaluated key structural parameters of the C–S–H including: chain length (CL) in Fig. 7(b); silicate chain length (SiCL) in Fig. 7(d); and Al/Si molar ratio for Al are incorporated into silicate chains of the C-S-H structure in Fig. 7(c). Drying does not appear to substantially influence the chain length for any of the binders, as moderate drying alone does not significantly reorganize the silicate network. After carbonation, the OPC system shows a notable increase in CL, consistent with the earlier observation of enhanced Q^2 connectivity. In the 30C system, CL could not be calculated for the 30C4MC sample because extensive decalcification of the C-A-S-H leads to the complete loss of the Q^1 environment. For 30CLC, chain length increases after carbonation, again reflecting the development of more polymerized silicate structures. For OPC and 30C, carbonation results in an increase in the Al/Si ratio, suggesting greater incorporation of Al into the silicate chains. In contrast, 30CLC shows a reduction in Al/Si after carbonation, pointing to a different carbonation pathway and possibly a more selective decalcification process. Silicate chain length (SiCL) increases after carbonation across all binders; however, the increase is most pronounced for the 30CLC system, in line with its greater structural polymerization observed in the ^{29}Si spectra.

To complement the structural interpretation from the NMR spectra, the level of decalcification (L_d) was quantified and given in Fig. 7(e). OPC 4MC exhibited L_d of 9%, indicating moderate decalcification in comparison to 30C which reached L_d of 92%, confirming that the C–S–H in 30C is highly vulnerable to Ca depletion, leading to extensive restructuring of the silicate network. 30CLC however, showed a L_d of 34% and thus much lower than 30C, despite being higher than OPC, reflecting the protective effect of extended curing. [56].

A semi-quantitative evaluation of silicate polymerization is presented in Fig. 7(f). The 30C binder shows a B/A ratio of 9.29, reflecting an extensive increase in silicate polymerization that aligns with its very high level of decalcification. In contrast, 30CLC exhibits a much lower B/A ratio of 1.32, indicating only limited polymerization, which is consistent with its substantially reduced degree of decalcification.

4.3. Effect of structural changes of C–A-S–H on re-distribution of Al

The ^{27}Al MAS NMR of the undried, 4MR and 4MC samples for OPC, 30C and 30CLC samples are shown in Fig. 8, Fig. 9 and Fig. 10. As expected, aluminum in octahedral coordination (Al^{VI}) is observed in the chemical shift range of 0–20 ppm, while tetrahedrally coordinated aluminum (Al^{IV}) appears between 50 and 90 ppm [61]. In all samples, sharp resonances at ~10 ppm and ~ 15 ppm are attributed to AFm [62] and AFt phases, respectively.

4.3.1. AFm and AFt at prior to carbonation stage

The undried OPC sample displays broad Al^{IV} peak centered at 60 and 71 ppm (Fig. 8a) reflects moderate Al incorporation into the C-A-S-H gel. Also, it displays a strong Al^{VI} signal (Fig. 8b), consistent with the presence of AFm and AFt phases at early hydration. In the undried 30C (Fig. 8a) sample, the Al^{VI} intensity is even higher than in OPC, reflecting rapid formation of AFm/AFt from the reactive fraction of activated-clay [76]. This aligns with the high early Al/Si ratio (0.16) and the dominant Q^2(1Al) contribution in the ^{29}Si spectrum. In contrast, the undried 30CLC sample exhibits a more balanced distribution between Al^{VI} and Al^{IV}, suggesting that extended hydration promotes gradual transformation of AFm into Al-incorporated C-A-S-H.

4.3.2. Effect of drying on AFm and AFt de-coupled from carbonation

In the 4MR condition, both binders largely preserve the aluminum coordination environments observed in the undried state, indicating that drying at 57% RH introduces only limited structural alteration. OPC remains dominated by Al^{VI}, reflecting the continued presence of AFm and AFt phases, while the broad Al^{IV} signal around 60–70 ppm shows only minor changes.

The 30C sample similarly retains its strong Al^{VI} contribution, consistent with the continued influence of activated-clay on AFm formation. The Al^{IV} region becomes marginally more defined, but the overall balance between Al^{VI} and Al^{IV} remains close to that of the undried state. This is in line with the small drop in Al/Si ratio and the largely unchanged chain length, confirming that moderate drying does not significantly disturb Al incorporation in 30C.

For 30CLC the Al^{VI} (Fig. 10b) and Al^{IV} (Fig. 9b) distribution remains more even, reflecting the more mature hydrate assemblage produced by extended curing. Only subtle reductions in Al^{VI} intensity appear after drying, accompanied by minimal changes in the Al^{IV} envelope. These trends are consistent with the very stable Al/Si ratio and chain length derived from the ^{29}Si spectra.

4.3.3. Effect of carbonation on AFm and AFt coupled with drying

Upon carbonation, both binders show a clear shift in Al coordination as the intensity of octahedral Al^{VI} is markedly reduced, and in the case of 30C it disappears entirely. The complete loss of Al^{VI} in 30C indicates that the remaining AFm/AFt phases are fully destabilized, which is consistent with the expected breakdown of ettringite once the pore solution pH falls below 10 [20]. This interpretation is supported by the accompanying XRD and TGA results, both of which show the disappearance of AFt after carbonation. The depletion of Al^{VI} and the simultaneous rise in tetrahedral Al^{IV} is in line with earlier observations by Skibsted et al. [63], who reported that carbonation drives the conversion of Al^{VI} to Al^{IV}, promoting Al incorporation into the silicate chains of C-A-S-Hor the formation of poorly crystalline aluminosilicate gels.

Carbonation also produces a modest but systematic shift of the Al^{IV} resonances toward lower chemical shifts appearing at ~58 and 68 ppm in OPC (Fig. 8a), ~58 ppm in 30C (Fig. 9a), and ~ 59, 68, and 74 ppm in 30CLC (Fig. 9b). Such shifts are typically associated with changes in local Al environments toward more disordered, gel-like aluminosilicate structures [56,64]. The increased Al^{IV} intensity after carbonation, observed consistently in all systems, further indicates that tetrahedrally coordinated Al becomes increasingly integrated into the reorganized silicate framework as decalcification progresses.

This evolution in the ^{27}Al spectra mirrors the trends seen in the ^{29}Si MAS NMR data, where carbonation enhances chain polymerization and promotes the formation of Q^3 and Q^4 environments. Together, the Si and Al NMR signatures point to a coupled decalcification–repolymerization process in which the loss of Ca not only collapses AFm/AFt phases but also redistributes Al into the silicate network, giving rise to more polymerized C-A-S-H or secondary aluminosilicate gels.

Owing to relatively lower availability of aluminum content in low kaolinite mix layer activated-clays, the 30C and 30CLC systems, have limited formation of AFm phases, which are known to act as an initial carbonation buffer by preferentially reacting with CO_2. The lower abundance of AFm consequently accelerates the exposure of the C-A-S-H phase to carbonation [5,63]. This reduced CO_2 buffering capacity allows

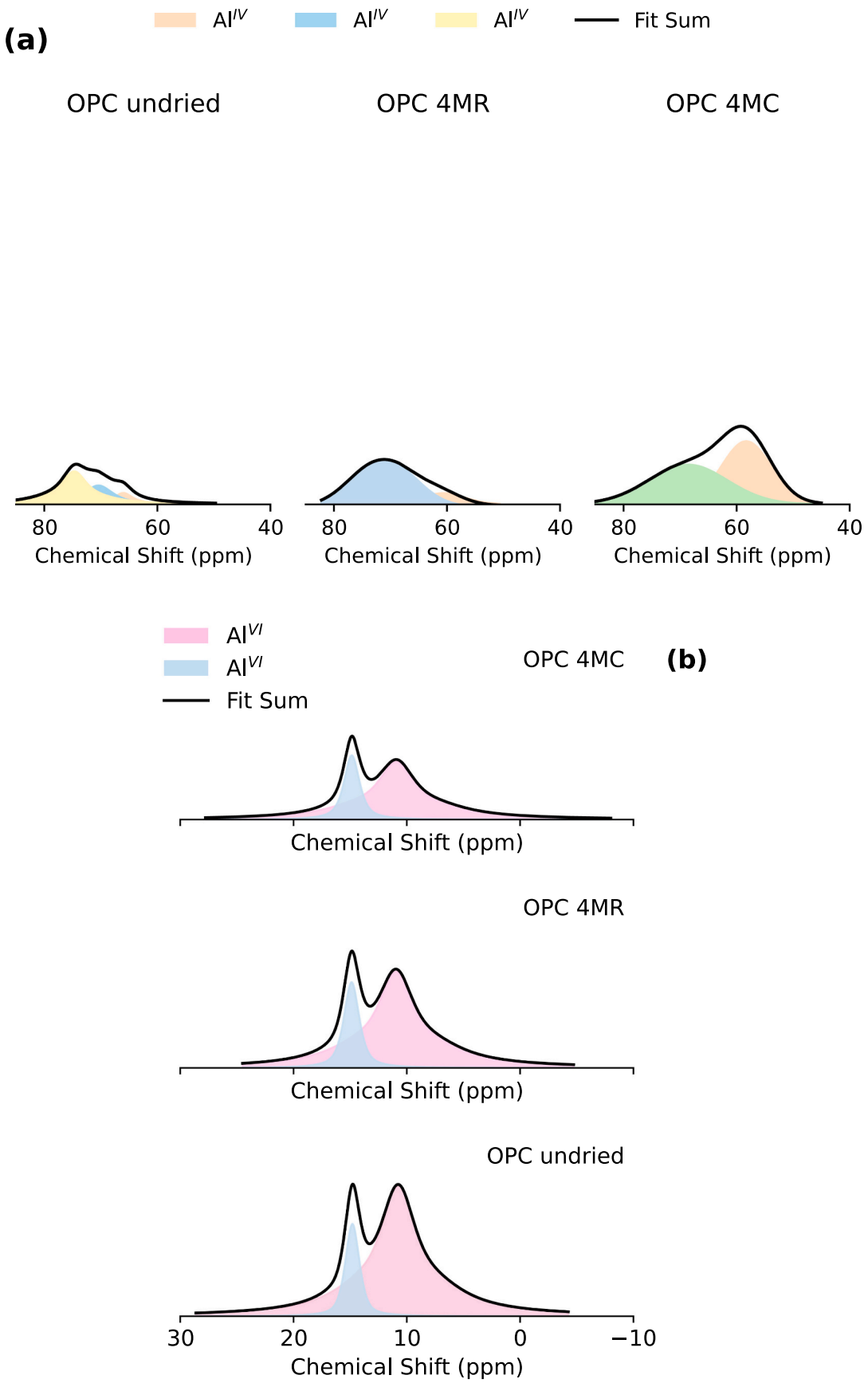

Fig. 8. 27Al MAS NMR spectra (a) Al^{IV} for OPC undried, uncarbonated and carbonated samples (b) Al^{VI} for OPC undried, uncarbonated and carbonated samples.

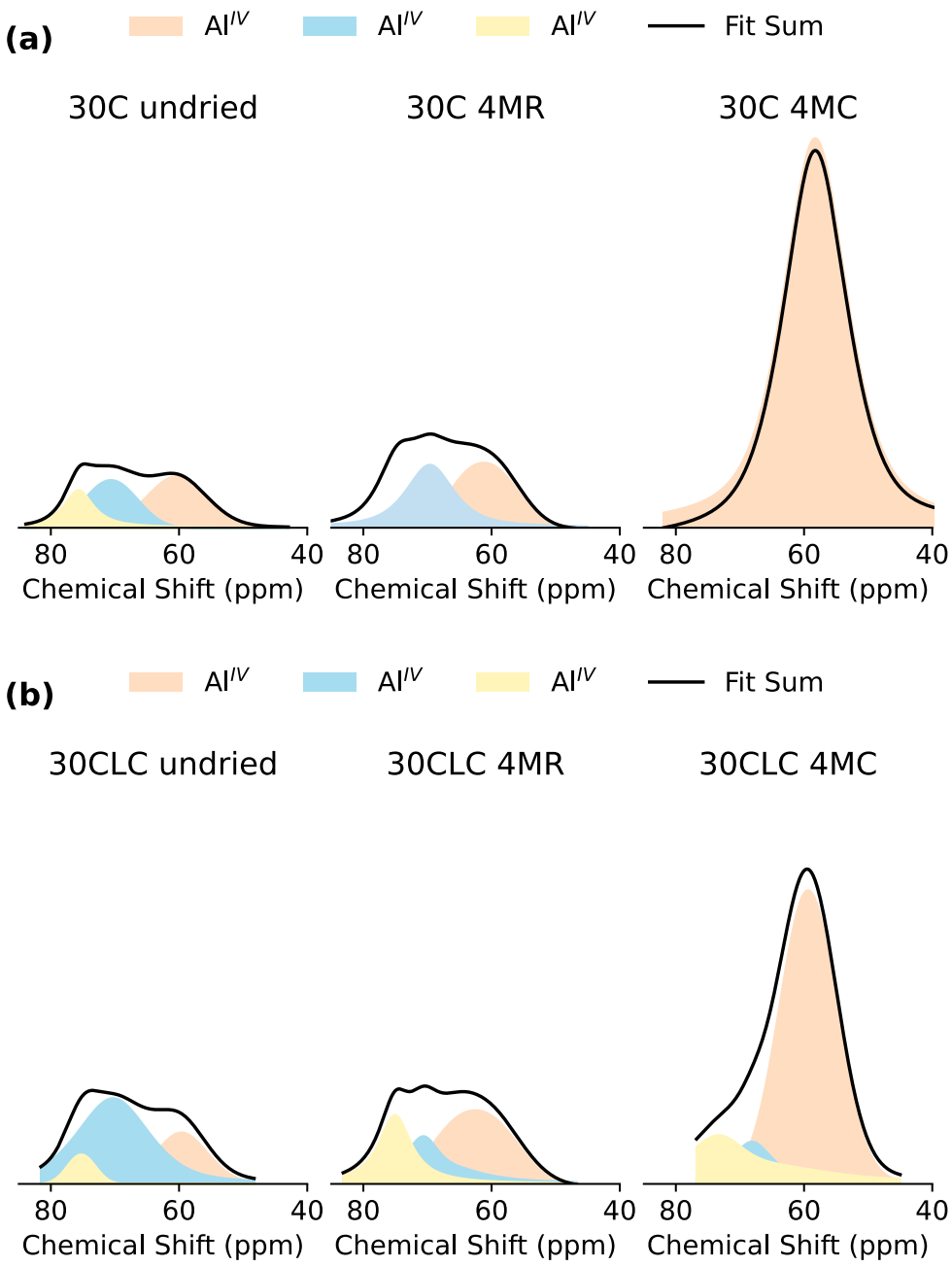

Fig. 9. ^{27}Al MAS NMR spectra (a) Al^{IV} for 30C undried, uncarbonated and carbonated samples (b) Al^{IV} for 30CLC undried, uncarbonated and carbonated samples.

carbonation to proceed more rapidly toward the decalcification and structural reorganization of the silicate chains, as confirmed by the evolution of Q^3 and Q^4 species in the ^{29}Si NMR spectra and the increase in tetrahedrally coordinated Al in ^{27}Al NMR. It is also important to take into consideration the role of curing duration for the activated-clay blended binder in carbonation resistance. 30C (28 days cured samples) exhibited a sharper decline in Al^{VI} and more pronounced silicate chain reorganization compared to 30CLC. The extended curing period allowed better hydration of activated-clay and formation of C-A-S-H and Afm phases, which improved the ability of matrix to resist carbonation. This contrasts with kaolinitic (1:1) activated clays, such as metakaolin, which release substantially higher amounts of reactive Si and Al during hydration-up to four times more silicon and twelve times more aluminum than montmorillonite [65]. The higher Al availability in such systems promotes AFm formation and Al^{IV} incorporation into C-A-S-H, leading to greater silicate chain polymerization and a more cross-linked aluminosilicate network that enhances resistance to carbonation [3,66].

4.4. *Effect of carbonation on re-distribution of pore structure*

Fig. 11 gives normalized mercury intrusion porosimetry (MIP) results showing the relative pore size distribution within each sample and Fig. 12, shows differential pore volumes across different exposure durations (1, 4, and 6 months).

4.4.1. *Effect of drying de-coupled from carbonation on re-distribution of pore structure*

Under drying conditions, in OPC, the fraction of small capillary pores (0.01–0.1 μm) gradually increases from 1 to 6 months, while the gel pore fraction with range < 0.01 μm slightly decreases. This indicates a slight coarsening of the pore structure during prolonged drying, likely caused by shrinkage of the C-S-H gel. As moisture is lost, part of the gel porosity

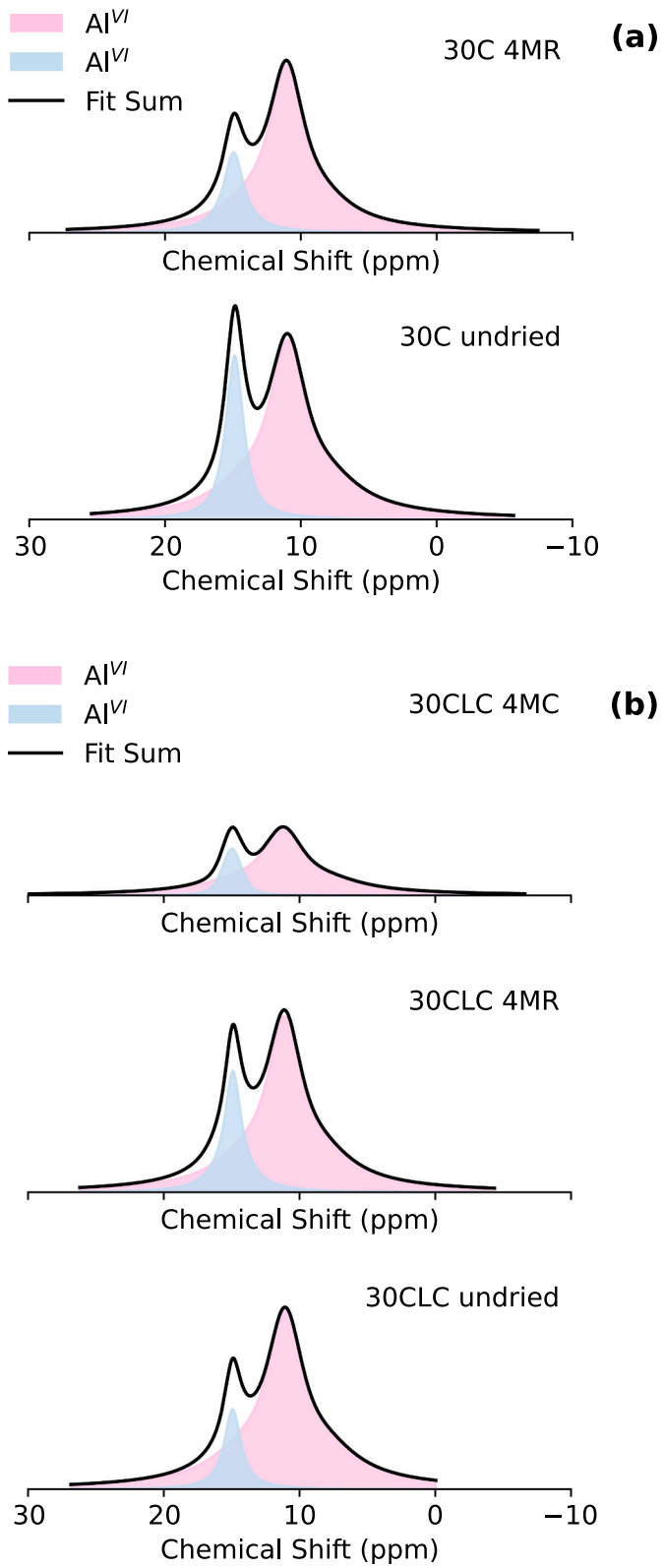

Fig. 10. 27Al MAS NMR (a) Al^{VI} for 30C undried and uncarbonated (b) Al^{VI} for 30CLC undried, uncarbonated and carbonated samples.

may transform into slightly larger capillary pores due to microstructural rearrangement and partial pore merging. The proportion of pores larger than 1 μm remains very small throughout.

In the case of 30C, the overall pattern resembles that of OPC, though the system generally contains a higher share of capillary pores, reflecting its coarser and more open microstructure at 28 days of curing.

For 30CLC, the fraction of gel pores is slightly higher, and capillary pores are less prominent compared to OPC and 30C. This reflects that extended curing resulted in continued pozzolanic activity leading to a denser pore structure, and more cohesive gel network that better resists coarsening.

4.4.2. Effect of carbonation coupled with drying on re-distribution of pore structure

A clear reduction in total porosity is observed in OPC after carbonation in comparison with reference samples in the same temperature and RH conditions as shown in Fig. 11d. The reduction in porosity is attributed to carbonation of portlandite, as the molar volume of calcium carbonated is higher than that of portlandite, irrespective of the type of polymorph of calcium carbonate precipitate [67]. Therefore, the additional solid volume fills the empty pore volume in the microstructure which results in reduction of overall porosity. In contrast, the 30C system the carbonated sample exhibits a slightly higher cumulative pore volume than the reference. This supports the idea that the limited availability of portlandite in activated-clay systems shifts carbonation toward the decalcification of C-S-H, potentially coarsening the pore structure instead of refining it [27,68–70]. For 30CLC, the difference in total pore volume between 6MR and 6MC is minimal. This reflects the fact that prolonged curing has already resulted in a relatively dense microstructure through continued hydration and pore filling, thereby limiting the extent of further densification induced by carbonation.

In the case of OPC, carbonation causes a clear shift toward finer pores. The fraction of gel pore volume (Fig. 11a) increases after carbonation while the proportion of small capillary pores (0.01–0.1 μm) decreases [71]. This trend is consistent throughout all exposure durations i.e. 1, 4, and 6 months. The reduction observed in small capillary pore range corresponds to partial clogging of pores corresponding to medium capillary pores, which are associated with outer C-S-H clusters [34,72] as reported in literature [73]. The increase in gel pores after carbonation can be attributed to the release of chemically bound water during carbonation, which, along with moisture available at the carbonation front, may facilitate continued hydration of unreacted clinker phases. As a result, the formation of additional C–S–H could contribute to the observed rise in gel porosity.

Moreover, as portlandite dissolves during carbonation, it leaves voids that can locally merge into slightly larger pores, while carbonation products preferentially precipitate within the finer pore ranges [17]. This simultaneous formation and filling process explains the appearance of new pores around 0.1–0.2 μm and the reduction in those near 0.03 μm, as also seen in the differential intrusion curves in Fig. 12.

In comparison with OPC, the activated-clay blended binders exhibited somewhat different responses. Although, in case of both 30C and 30CLC the volume of small capillary pores (0.01–0.1 μm) decreases consistently after carbonation across all exposure durations, yet the proportion of medium capillary pores (0.1–1 μm) increases, which reflects coarsening of porosity. Although the total porosity in 30CLC remains almost the same between the 30CLC 6MR and 30CLC 6MC samples, the internal pore size distribution still indicates coarsening. Previous studies have reported that carbonation can lead to coarsening of mesopores, mainly due to the formation of porous silica gel, microcracking in the $CaCO_3$ layer around portlandite, and shrinkage-induced cracking. This effect is particularly evident in binders with low Ca/Si ratios, such as those containing fly ash, slag, or silica fume, where limited portlandite and the decalcification of C-A-S-H promote higher porosity and a shift toward larger pores [28,74].

As confirmed by the TGA results, carbonation in 30C and 30CLC proceeds beyond portlandite consumption and involves the carbonation of sulfoaluminate hydrates (AFt and AFm) [20,55]. Following the early exhaustion of CH in these systems, the destabilisation and decomposition of these pore-filling phases contribute directly to the observed pore coarsening. In addition to C-A-S-H decalcification, carbonation of

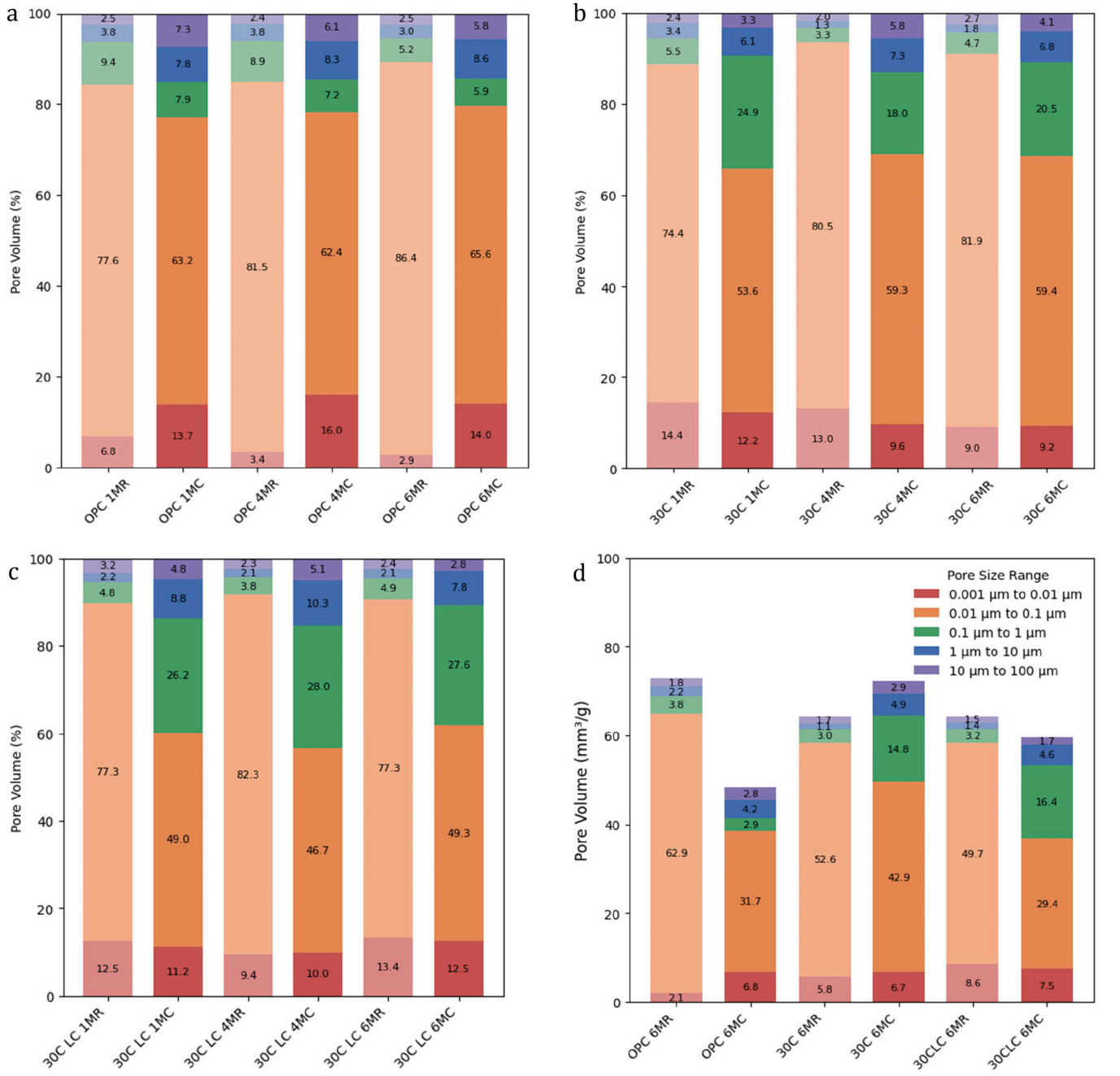

Fig. 11. Mercury intrusion porosimetry – Pore structure evolution under drying and carbonation (a) OPC over 1, 4 and 6 months of age (b) 30C over 1, 4 and 6 months of age (c) 30CLC over 1, 4 and 6 months of age (d) Total porosity of OPC, 30C and 30CLC. Values represent the average of two measurements.

ettringite (AFt) plays an important role in microstructural evolution. Ettringite is a highly voluminous, pore-filling hydrate, and its destabilisation during carbonation leads to dissolution and partial replacement by calcite, gypsum, and Al-rich amorphous phases [55]. The dissolution of AFt locally increases pore volume and pore connectivity, particularly within the capillary and mesopore ranges.

Similarly, carbonation of AFm phases reduces their pore-filling efficiency through progressive decalcification and transformation into carbonate-bearing or Al-rich residual phases. Although some carbonation products may precipitate within finer pores, the net effect of AFt and AFm decomposition is a redistribution of porosity toward the medium capillary pore range (0.1–1 µm), consistent with the MIP results for both 30C (Fig. 11b) and 30CLC (Fig. 11c) [55]. This mechanism is particularly relevant in systems with limited portlandite availability, where early CH exhaustion accelerates sulfoaluminate carbonation and promotes pore coarsening even when changes in total porosity are small, as observed for 30CLC. The involvement of AFt and AFm carbonation is further supported by the NMR results, which showed structural changes associated with aluminate-bearing hydrates during carbonation.

In 30C, the gel-pore fraction (<0.01 µm) remains almost unchanged, which leads to the idea that no later hydration is going on in 30C. On the other hand, 30CLC shows a slight increase in gel pores, especially in the 6-month carbonated sample. This could be related to secondary hydration supported by the moisture available during carbonation. Studies have reported that the decrease in micro-pores is attributed to clogging by $CaCO_3$ from C–S–H carbonation, while the reduction of macro-pores is mainly attributed to pore clogging by $CaCO_3$ from portlandite carbonation [17,20,68,75].

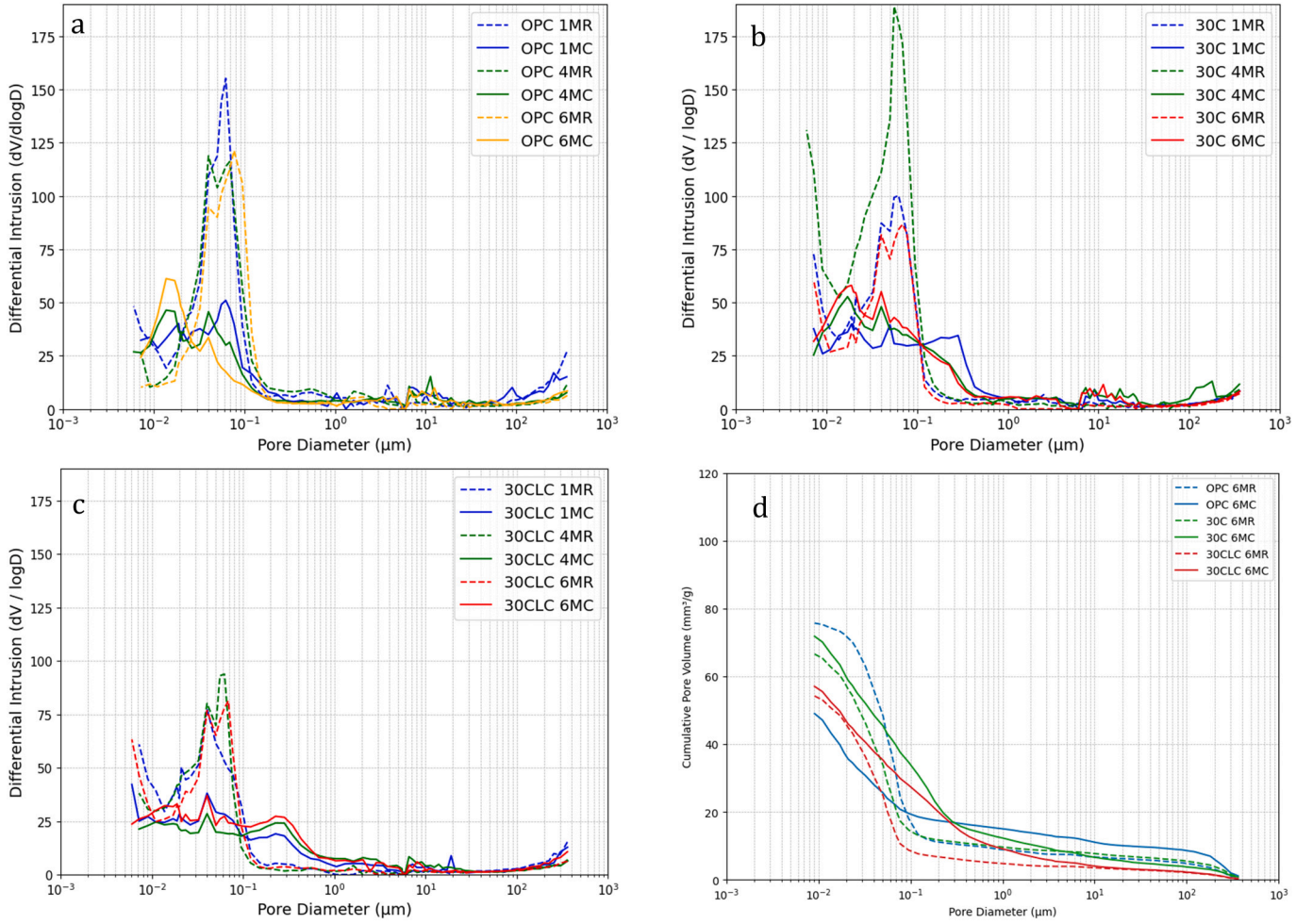

Fig. 12. Mercury intrusion porosimetry – Differential porosity under drying and carbonation (a) OPC over 1, 4 and 6 months of age (b) 30C over 1, 4 and 6 months of age (c) 30CLC over 1, 4 and 6 months of age (d) Cumulative pore volume of OPC, 30C and 30CLC.

Further insight into microstructural evolution is provided by the differential intrusion curves shown in Fig. 12. In the reference (MR) samples, two distinct peaks appear within the 0.01–0.1 μm range, which correspond to the medium capillary pores typically associated with outer C–S–H clusters [76]. Upon carbonation, the intensity of these peaks decreases in all three binder systems, indicating partial blockage and densification of the capillary network. In some cases, the main peak shifts slightly toward smaller diameters, suggesting mild pore refinement [77].

5. Mechanistic reflections and implications for carbonation in low-kaolinite 2:1 activated-clay binders

The results presented above show that carbonation behavior in low-kaolinite 2:1 activated-clay blended binders cannot be fully rationalised using durability concepts established for OPC or kaolinite-rich LC^3 systems. This section therefore integrates the experimental observations to elucidate the governing mechanisms, with particular emphasis on the carbonation buffering sequence, the role of C-A-S-H chemistry, and the influence of moisture-induced microstructural conditioning. The aim is not to restate individual findings, but to provide a coherent mechanistic interpretation of the observed carbonation response.

In OPC systems, carbonation resistance is primarily governed by portlandite buffering, whereas in LC^3 binders a substantial fraction of reactive aluminum promotes the formation of carboaluminate (AFm) phases that provide sustained intermediate CO_2 buffering once CH is depleted. In contrast, the low-kaolinite 2:1 activated-clay binder investigated here contains limited amounts of both CH and AFm. As a result, carbonation proceeds through a distinct buffering sequence: initial consumption of the available portlandite, followed by a brief and limited AFm contribution, before progressing relatively early toward interaction with the C-A-S-H gel. This altered buffering hierarchy implies that carbonation damage is controlled less by the quantity of classical buffering phases and more by the behavior of the gel once these phases are exhausted.

The comparison between the short-cured (30C) and extended-cured (30CLC) systems illustrates this shift clearly. Extended curing does not increase portlandite content, which remains similar or slightly reduced due to continued pozzolanic consumption. Nevertheless, carbonation damage differs markedly. In 30C, carbonation of a chemically immature C-A-S-H leads to extensive decalcification, strong silicate reorganization toward Q^3/Q^4 environments, and pronounced pore coarsening (Ld ≈ 92%). In contrast, 30CLC exhibits substantially reduced decalcification (Ld ≈ 34%), consistent with greater aluminum incorporation and higher silicate connectivity within the gel. These differences demonstrate that curing primarily alters the chemical state of C-A-S-H rather than the overall buffering capacity of the binder.

Drying experiments provide essential context for interpreting these effects. Exposure to 57% RH produces measurable changes in pore structure, including contraction of the gel and redistribution of fine pores toward slightly larger sizes. These changes indicate loss of interlayer and gel water and partial physical rearrangement of the C-A-S-H structure. Importantly, however, drying alone does not induce substantial decalcification or the extensive silicate reorganization observed

under carbonation. This shows that physical pore restructuring and gel contraction can occur without chemical degradation of the hydrate assemblage.

At the same time, the drying results demonstrate that the microstructure and internal state of the gel prior to carbonation are not static. Drying modifies pore connectivity and gel packing, thereby influencing transport properties and the local moisture conditions under which carbonation occurs. Carbonation then acts on this conditioned microstructure: chemical decalcification of C-A-S-H amplifies and stabilises pore coarsening that would otherwise remain limited or potentially reversible under drying alone. In this sense, carbonation does not simply reproduce drying-induced changes but builds upon them through irreversible chemical transformation of the gel.

This coupling between moisture state and carbonation is particularly important for low-buffer systems such as low-kaolinite activated-clay binders. Because classical buffering phases are limited, variations in internal relative humidity influence not only CO_2 transport but also the physical condition of the C-A-S-H at the onset of carbonation. Changes in exposure RH may therefore modulate carbonation damage by controlling the extent of drying-induced gel contraction prior to chemical attack. This highlights moisture history as a relevant parameter alongside binder chemistry in assessing carbonation resistance.

Within this combined framework, C-A-S-H emerges as the central phase governing carbonation behavior in low-kaolinite systems. Once CH and AFm phases are depleted, the degree of aluminum incorporation and silicate connectivity determines whether carbonation results in limited restructuring or extensive gel collapse. Curing duration influences this response by enabling gradual chemical evolution of the gel, while drying controls its physical conditioning. The selected activated-clay replacement level (30%) allows these interactions to be observed clearly; at higher replacement levels, carbonation would likely proceed directly to gel decalcification, further increasing the importance of gel chemistry and moisture state.

6. Conclusions

This study investigated carbonation in low kaolinite mixed layer activated-clay blended binders, focusing on hydrate phase evolution, C-A-S-H structure, and pore characteristics, while separating the influences of curing, drying, and carbonation. The following conclusions are drawn:

1. Carbonation in low kaolinite 2:1 activated-clay binders follows a mechanism distinct from OPC and kaolinite rich LC^3 systems: limited portlandite and AFm availability lead to an altered carbonation buffering sequence, with early interaction between CO_2 and the C-A-S-H gel. As a result, carbonation resistance cannot be assessed based on portlandite content alone.
2. The chemical state of C-A-S-H governs the severity of carbonation damage once buffering phases are depleted: chemically immature gels exhibit extensive decalcification, silicate reorganization (Q^3/Q^4), and severe pore coarsening (Ld $\approx$ 92%), whereas gels with higher aluminum incorporation and greater silicate connectivity show substantially reduced decalcification and improved microstructural stability (Ld $\approx$ 34%).
3. Drying induces physical pore restructuring and gel contraction without causing deep chemical degradation: exposure to 57% RH leads to redistribution of fine pores and limited silicate rearrangement, demonstrating that C-A-S-H can accommodate physical changes associated with moisture loss without structural collapse.
4. Carbonation acts as a chemical magnifier of prior microstructural conditioning rather than a simple extension of drying effects: severe pore coarsening observed under carbonation arises from chemically driven decalcification of C-A-S-H and cannot be explained by drying alone. Carbonation stabilises and amplifies pore changes that are otherwise limited under drying conditions.
5. Curing duration and moisture history jointly influence carbonation response in low kaolinite activated-clay binders: curing governs the chemical evolution of C-A-S-H, while drying controls its physical state and pore structure prior to carbonation. Both factors condition the subsequent carbonation pathway and extent of damage.

Taken together, these conclusions clarify the governing mechanisms of carbonation in low-kaolinite activated-clay binders; however, their broader applicability and practical implementation require further consideration. This study is limited to a single natural low-kaolinite 2:1 mixed-layer activated-clay and therefore represents one manifestation of a broader class of low-Al activated-clay-based binder systems. While such systems inherently form modest amounts of AFm and a chemically distinct C-A-S-H that governs carbonation buffering, future work should explore whether binder design strategies can deliberately alter hydrate assemblage development, for example by promoting greater AFm formation or modifying aluminum partitioning between AFm and C-A-S-H-rather than relying on extended curing alone. In parallel, the coupled effect of relative humidity and carbonation requires further investigation, as moisture-induced conditioning of the hydrate assemblage and pore structure is expected to interact strongly with subsequent carbonation reactions and damage evolution in low-buffer activated-clay-based binders. It should also be noted that, in this study, AFm phases are treated as a combined group, whereas in more detailed or follow-up studies, characterizing the specific carbonation pathways involving individual AFm phases can provide valuable insight.

CRediT authorship contribution statement

Sahar Iftikhar: Writing – review & editing, Writing – original draft, Methodology, Investigation, Formal analysis, Data curation. **Ingemar Löfgren:** Writing – review & editing, Supervision. **Joao Figueira:** Investigation, Formal analysis, Data curation. **Helen Jansson:** Writing – review & editing, Investigation, Formal analysis, Data curation. **Jelke Dijkstra:** Writing – review & editing, Supervision. **Arezou Babaahmadi:** Writing – review & editing, Supervision, Project administration, Methodology, Funding acquisition, Conceptualization.

Declaration of competing interest

The authors declare that they have no known competing financial interests or personal relationships that could have appeared to influence the work reported in this paper.

Acknowledgements

The authors acknowledge the grant offered by Family Thomas Foundation for project: Evolution of pozzolan incorporated concrete: resistance to carbonation (Carbo-crete). The authors gratefully acknowledge Luping Tang and Karin Lundgren for their insightful feedback on the manuscript. The authors would like to acknowledge NMR support from the NMR Core Facility at the Swedish NMR Centre (SwedNMR, Umeå node), Umeå University and SciLifeLab. We thank Amrita Hazarika for providing undried hydrated raw data for TGA and NMR. Additionally, the authors are grateful to Haitao Gu for facilitating the MIP measurements, and student assistants at Chalmers Building Materials Lab – Archanath Dickwella, Sunil Gautam, Suriyaprakash Saravanan and Amith Adhikari for helping with material preparations and experiments.

Appendix A. Supplementary data

Supplementary data to this article can be found online at https://doi.org/10.1016/j.cemconres.2026.108322.

Data availability

Data will be made available on request.

References

[1] K.L. Scrivener, V.M. John, E.M. Gartner, Eco-efficient cements: potential economically viable solutions for a low-CO2 cement-based materials industry, Cem. Concr. Res. 114 (2018) 2–26.
[2] R. Snellings, P. Suraneni, J. Skibsted, Future and emerging supplementary cementitious materials, Cem. Concr. Res. 171 (2023) 107199.
[3] F. Avet, K. Scrivener, Investigation of the calcined kaolinite content on the hydration of limestone calcined clay cement (LC3), Cem. Concr. Res. 107 (2018) 124–135.
[4] R. Fernandez, F. Martirena, K.L. Scrivener, The origin of the pozzolanic activity of calcined clay minerals: a comparison between kaolinite, illite and montmorillonite, Cem. Concr. Res. 41 (1) (2011) 113–122.
[5] K. Scrivener, et al., Calcined clay limestone cements (LC3), Cem. Concr. Res. 114 (2018) 49–56.
[6] F. Avet, K. Scrivener, Influence of pH on the chloride binding capacity of limestone calcined clay cements (LC3), Cem. Concr. Res. 131 (2020) 106031.
[7] N. Beuntner, R. Sposito, K.-C. Thienel, Potential of calcined mixed-layer clays as pozzolans in concrete, ACI Mater. J. 116 (4) (2019) 19–29.
[8] A. Ahlberg, I. Olsson, P. Šimkevičius, Triassic–Jurassic weathering and clay mineral dispersal in basement areas and sedimentary basins of southern Sweden, Sediment. Geol. 161 (1–2) (2003) 15–29.
[9] G. Plusquellec, A. Babaahmadi, U. Mueller, Activated Clays as Supplementary Cementitious Material, 2021.
[10] Y. Dhandapani, et al., The meta-kaolinite content of the calcined clay source impacts the mechanical and durability performance of blended Portland concrete, Cem. Concr. Res. 196 (2025) 107922.
[11] M. Setti, et al., Clay mineralogy in southern Africa river muds, Clay Miner. 49 (5) (2014) 717–733.
[12] M. Flegar, et al., Regional waste streams as potential raw materials for immediate implementation in cement production, Materials 13 (23) (2020) 5456.
[13] I. Tole, Enhancing the Pozzolanic activity of three natural clays from Sweden by Mechanochemical activation process, Available at SSRN 4100172 (2022).
[14] A. Alujas, et al., Pozzolanic reactivity of low grade kaolinitic clays: influence of calcination temperature and impact of calcination products on OPC hydration, Appl. Clay Sci. 108 (2015) 94–101.
[15] A.T. Marsh, S. Krishnan, S.A. Bernal, Structural features of thermally or mechano-chemically treated montmorillonite clays as precursors for alkali-activated cements production, Cem. Concr. Res. 181 (2024) 107546.
[16] A. Hazarika, et al., Evolution of hydration in cement blends with incorporation of activated low-kaolinite clays: insights into the preferred aluminum uptake by C-(a)-SH, Cem. Concr. Res. 201 (2026) 108086.
[17] B. Wu, G. Ye, Development of porosity of cement paste blended with supplementary cementitious materials after carbonation, Constr. Build. Mater. 145 (2017) 52–61.
[18] M.A. Peter, et al., Competition of several carbonation reactions in concrete: a parametric study, Cem. Concr. Res. 38 (12) (2008) 1385–1393.
[19] V. Ngala, C. Page, Effects of carbonation on pore structure and diffusional properties of hydrated cement pastes, Cem. Concr. Res. 27 (7) (1997) 995–1007.
[20] S. von Greve-Dierfeld, et al., Understanding the carbonation of concrete with supplementary cementitious materials: a critical review by RILEM TC 281-CCC, Mater. Struct. 53 (6) (2020) 136.
[21] D.J. Anstice, C.L. Page, M.M. Page, The pore solution phase of carbonated cement pastes, Cem. Concr. Res. 35 (2) (2005) 377–383.
[22] J. Visser, Influence of the carbon dioxide concentration on the resistance to carbonation of concrete, Constr. Build. Mater. 67 (2014) 8–13.
[23] J. Chang, Y. Fang, Quantitative analysis of accelerated carbonation products of the synthetic calcium silicate hydrate(C–S–H) by QXRD and TG/MS, J. Therm. Anal. Calorim. 119 (1) (2015) 57–62.
[24] V. Lilkov, et al., Long term study of hardened cement pastes containing silica fume and fly ash, Construct. Build Mater. 60 (2014) 48–56 (Constr. Build. Mater.).
[25] H. El-Hassan, Y. Shao, Early carbonation curing of concrete masonry units with Portland limestone cement, Cem. Concr. Compos. 62 (2015) 168–177.
[26] P.H.R. Borges, et al., Carbonation of CH and C–S–H in composite cement pastes containing high amounts of BFS, Cem. Concr. Res. 40 (2) (2010) 284–292.
[27] A. Morandeau, M. Thiéry, P. Dangla, Impact of accelerated carbonation on OPC cement paste blended with fly ash, Cem. Concr. Res. 67 (2015) 226–236.
[28] S.T. Pham, W. Prince, Effects of carbonation on the microstructure of cement materials: influence of measuring methods and of types of cement, Int. J. Concr. Struct. Mater. 8 (4) (2014) 327–333.
[29] K. Sisomphon, L. Franke, Carbonation rates of concretes containing high volume of pozzolanic materials, Cem. Concr. Res. 37 (12) (2007) 1647–1653.
[30] A. Morandeau, M. Thiery, P. Dangla, Investigation of the carbonation mechanism of CH and CSH in terms of kinetics, microstructure changes and moisture properties, Cem. Concr. Res. 56 (2014) 153–170.
[31] L. Black, et al., Structural features of C–S–H (I) and its carbonation in air—a Raman spectroscopic study. Part II: carbonated phases, J. Am. Ceram. Soc. 90 (3) (2007) 908–917.
[32] F. Georget, J.H. Prévost, B. Huet, Impact of the microstructure model on coupled simulation of drying and accelerated carbonation, Cem. Concr. Res. 104 (2018) 1–12.
[33] W. Soja, et al., Evolution of microstructural changes in cement paste during environmental drying, Cem. Concr. Res. 134 (2020) 106093.
[34] H.-W. Song, S.-J. Kwon, Permeability characteristics of carbonated concrete considering capillary pore structure, Cem. Concr. Res. 37 (6) (2007) 909–915.
[35] M. Auroy, et al., Impact of carbonation on unsaturated water transport properties of cement-based materials, Cem. Concr. Res. 74 (2015) 44–58.
[36] A. Hazarika, L. Huang, A. Babaahmadi, Characterisation, activation, and reactivity of heterogenous natural clays, Mater. Struct. 57 (4) (2024) 68.
[37] Standardization, E.C.f, EN 12390–12:2020 — Testing hardened concrete – Part 12: Determination of the carbonation resistance of concrete: Accelerated carbonation method, 2020. Brussels, Belgium.
[38] K. De Weerdt, et al., Hydration mechanisms of ternary Portland cements containing limestone powder and fly ash, Cem. Concr. Res. 41 (3) (2011) 279–291.
[39] B.M.K. Fung, A. K., K. Ermolaev, An improved broadband decoupling sequence for liquid crystals and solids, J. Magn. Reson. 142 (2000) 97–101.
[40] T. O'Haver, ipf(arg1,arg2,arg3,arg4). MATLAB Central File Exchange, 2025. Retrieved June 24, 2025.
[41] Z. Dai, T.T. Tran, J. Skibsted, Aluminum incorporation in the C–S–H phase of white Portland cement–metakaolin blends studied by 27 Al and 29 Si MAS NMR spectroscopy, J. Am. Ceram. Soc. 97 (8) (2014) 2662–2671.
[42] W. Liu, et al., XRD and 29Si MAS NMR study on carbonated cement paste under accelerated carbonation using different concentration of CO2, Mater. Today Commun. 19 (2019) 464–470.
[43] B. Gonçalves, et al., X-ray diffraction study of the early hydration of Portland cements containing calcium carbonate by in-situ and ex-situ approaches, Construct. Build Mater. 365 (2023) 129947 (Constr. Build. Mater).
[44] B. Lu, et al., Effects of carbonated hardened cement paste powder on hydration and microstructure of Portland cement, Construct. Build Mater. 186 (2018) 699–708 (Constr. Build. Mater).
[45] D. Gastaldi, et al., Hydration products in sulfoaluminate cements: evaluation of amorphous phases by XRD/solid-state NMR, Cem. Concr. Res. 90 (2016) 162–173.
[46] R. Hay, L. Li, K. Celik, Shrinkage, hydration, and strength development of limestone calcined clay cement (LC3) with different sulfation levels, Cem. Concr. Compos. 127 (2022) 104403.
[47] F. Zunino, K. Scrivener, Microstructural developments of limestone calcined clay cement (LC3) pastes after long-term (3 years) hydration, Cem. Concr. Res. 153 (2022) 106693.
[48] F. Bahman-Zadeh, A.A. Ramezanianpour, A. Zolfagharnasab, Effect of carbonation on chloride binding capacity of limestone calcined clay cement (LC3) and binary pastes, J. Build. Eng. 52 (2022) 104447.
[49] B. Lothenbach, K. Scrivener, R. Hooton, Supplementary cementitious materials, Cem. Concr. Res. 41 (12) (2011) 1244–1256.
[50] Z. Huang, T. Liang, Experimental studies on durability performances of ultra-lightweight low-carbon LC3 cement composites against chloride ingression and carbonation, Constr. Build. Mater. 395 (2023) 132340.
[51] F. Deschner, et al., Hydration of Portland cement with high replacement by siliceous fly ash, Cem. Concr. Res. 42 (10) (2012) 1389–1400.
[52] J. Herterich, Microstructure and Phase Assemblage of Low-Clinker Cements during Early Stages of Carbonation, University of Leeds, 2017.
[53] M. Panzer, et al., An approach to estimate the strength contribution of calcined clays in blended cements, Construct. Build Mater. 447 (2024) 137800 (Constr. Build. Mater).
[54] E. Dubina, et al., Influence of water vapour and carbon dioxide on free lime during storage at 80 C, studied by Raman spectroscopy, Spectrochim. Acta A Mol. Biomol. Spectrosc. 111 (2013) 299–303.
[55] H. Yang, et al., Carbonation of ettringite and monosulfate: product evolution, microstructure, and comparison, Cem. Concr. Compos. 164 (2025) 106297.
[56] M. Auroy, et al., Comparison between natural and accelerated carbonation (3% CO2): impact on mineralogy, microstructure, water retention and cracking, Cem. Concr. Res. 109 (2018) 64–80.
[58] T.T.T. Zhuo Dai, Jørgen Skibsted, Aluminum Incorporation in the C–S–H Phase of White Portland Cement–Metakaolin Blends Studied by 27Al and 29Si MAS NMR Spectroscopy, 2014.
[59] Y. Ikeda, et al., 29Si MAS NMR study on structural change of silicate anions with carbonation of synthetic 11Å tobermorite, J. Ceram. Soc. Jpn. 100 (1165) (1992) 1098–1102.
[60] J. Skibsted, J. Hjorth, H.J. Jakobsen, Correlation between 29Si NMR chemical shifts and mean Si O bond lengths for calcium silicates, Chem. Phys. Lett. 172 (3–4) (1990) 279–283.
[61] F.M. Neto, R. Snellings, J. Skibsted, Aqueous carbonation of aged blended Portland cement pastes: impact of the Al/Si ratio on the structure of the alumina-silica gel, Cem. Concr. Res. 177 (2024) 107428.
[62] F.M. Neto, R. Snellings, J. Skibsted, Reactivity of aqueous carbonated cement pastes: effect of chemical composition and carbonation conditions, J. CO_2 Util. 89 (2024) 102970 (J. CO_2 Util.).
[63] F. Maia Neto, J. Skibsted, Characterization of aqueous carbonated cement-based materials by multinuclear solid-state NMR spectroscopy, J. Sustain. Cem.-Based Mater. 14 (6) (2025) 1191–1206.
[64] T.F. Sevelsted, J. Skibsted, Carbonation of C–S–H and C–a–S–H samples studied by 13C, 27Al and 29Si MAS NMR spectroscopy, Cem. Concr. Res. 71 (2015) 56–65.
[65] F. Souayfan, et al., 29Si and 27Al MAS NMR spectroscopic studies of activated metakaolin-slag mixtures, Construct. Build Mater. 322 (2022) 126415 (Constr. Build. Mater).

[66] R. Jaskulski, D. Jóźwiak-Niedźwiedzka, Y. Yakymechko, Calcined clay as supplementary cementitious material, Materials (Basel) 13 (21) (2020).
[67] B. Lagerblad, Carbon Dioxide Uptake during Concrete Life Cycle: State of the Art, Swedish Cement and Concrete Research Institute, Stockholm, 2005.
[68] V. Shah, et al., Changes in microstructure characteristics of cement paste on carbonation, Cem. Concr. Res. 109 (2018) 184–197.
[69] Z. Shi, et al., Experimental studies and thermodynamic modeling of the carbonation of Portland cement, metakaolin and limestone mortars, Cem. Concr. Res. 88 (2016) 60–72.
[70] G. Villain, M. Thiery, Impact of Carbonation on Microstructure and Transport Properties of Concrete. In Proceedings of, 2005.
[71] T. Chen, X. Gao, Effect of carbonation curing regime on strength and microstructure of Portland cement paste, J. CO_2 Util. 34 (2019) 74–86.
[72] H. Matsusato, et al., Studies on the carbonation of hydrated cement and its effect on microstructure and strength, in: In 9th International Congress on the Chemistry of Cement, National Council for Cement and Building Materials New Dehli, 1992.
[73] S. Pihlajavaara, Some results of the effect of carbonation on the porosity and pore size distribution of cement paste, Mater. Constr. 1 (6) (1968) 521–527.
[74] J.J. Chen, J.J. Thomas, H.M. Jennings, Decalcification shrinkage of cement paste, Cem. Concr. Res. 36 (5) (2006) 801–809.
[75] J.-S. Kim, et al., Effect of carbonation on cement paste microstructure characterized by micro-computed tomography, Construct. Build Mater. 263 (2020) 120079 (Constr. Build. Mater).
[76] J.F. Young, The Science and Technology of Civil Engineering Materials, No Title, 1998.
[77] R.A. Cook, K.C. Hover, Mercury porosimetry of hardened cement pastes, Cem. Concr. Res. 29 (6) (1999) 933–943.